Numerical study of Hawking radiation photosphere formation around microscopic black holes

James M. Cline and Michael Mostoslavsky
McGill University, Montréal, Québec, Canada H3A 2T8

Géraldine Servant*
Ecole Normale Supérieure de Lyon, Lyon, France
(Received 22 October 1998; published 25 February 1999)

Heckler has recently argued that the Hawking radiation emitted from microscopic black holes has sufficiently strong interactions above a certain critical temperature that it forms a photosphere, analogous to that of the Sun. In this case, the visible radiation is much cooler than the central temperature at the Schwarzschild radius, in contrast with the naive expectation for the observable spectrum. We investigate these ideas more quantitatively by solving the Boltzmann equation using the test particle method. We confirm that at least two kinds of photospheres may form: a quark-gluon plasma for black holes of mass $M_{BH} \lesssim 5\times 10^{14}$ g and an electron-positron-photon plasma for $M_{BH} \lesssim 2\times 10^{12}$ g. The QCD photosphere extends from the black hole horizon to a distance of 0.2–4.0 fm for 10^9 g$\lesssim M_{BH} \lesssim 5\times 10^{14}$ g, at which point quarks and gluons with average energy of order Λ_{QCD} hadronize. The QED photosphere starts at a distance of approximately 700 black hole radii and dissipates at about 400 fm, where the average energy of the emitted electrons, positrons and photons is inversely proportional to the black hole temperature, and significantly higher than was found by Heckler. The consequences of these photospheres for the cosmic diffuse gamma ray and antiproton backgrounds are discussed: bounds on the black hole contribution to the density of the universe are slightly weakened. [S0556-2821(99)03206-3]

PACS number(s): 97.60.Lf, 04.70.Dy, 95.30.Cq, 98.70.Rz

I. INTRODUCTION

It has long been known that black holes (BHs) are not perfectly black, but emit nearly blackbody radiation at a temperature $T_{BH}=(8\pi GM)^{-1}$ due to quantum mechanical effects [1] (where G is Newton's gravitational constant). Although this Hawking radiation is negligible for astrophysically large black holes, it becomes sufficiently hot to be visible for masses $M \lesssim 10^{15}$ GeV, corresponding to a BH that would be disappearing today, assuming it was present at the big bang. The present density of such BH's in the universe is in fact limited by observations of the diffuse gamma ray background coming from their accumulated radiation [2]. Such limits are calculated assuming Hawking's expression for the spectrum,

$$\frac{dN}{dEdt}=\frac{\sigma_s(E)E^2}{2\pi}\frac{1}{\exp(E/T_{BH})\pm 1} \tag{1}$$

where the sign depends on whether the emitted particle is a fermion (+) or a boson (−), and $\sigma_s(E)$ is the absorption cross section for the emitted particle, which depends on its spin s [3]. Moreover, previous estimates of the possibility of observing individual black holes, which explode in a burst of radiation as their masses approach to Planck mass, are also based on Eq. (1), combined with calculations of the mass spectrum of primordial black holes (PBH's) that could form during inflation [4] or the QCD phase transition [5], and guesses as to how they might cluster. It is possible that extremely high energy neutrinos from exploding PBH's will be observable in the new generation of neutrino telescopes [6].

Recently Heckler [7] revived the possibility that the spectrum (1) need not hold far away from the Schwarschild radius, $r_H=2GM$, because the radiation might interact with itself in some region, similar to photons diffusing inside the photosphere of the Sun. The idea had been previously dismissed [9,10], but in the framework of QED, Heckler identified bremsstrahlung and pair production as processes which could change this negative conclusion. Both interactions cause a small initial number of high energy particles to fragment into many lower energy particles, giving a significant decrease in the average particle energy. Consequently, according to Ref. [7], a BH with $T=45$ GeV at r_H would appear to an observer more like a BH with $T=m_e$ (the electron mass), in terms of average energy, but much brighter in terms of absolute luminosity.

As recognized by Heckler, it is not easy to give a highly quantitative treatment of the problem because, unlike in the Sun, the system is never so strongly coupled as to admit the approximation of local thermal equilibrium. The problem is that, whereas the sun has a huge chemical potential in gravitationally bound electrons and protons which are providing the large density, in the BH there are equal numbers of particles and antiparticles, which are at first freely streaming away from the horizon. The density at the horizon is $\sim T^3$ but quickly falls like $1/r^2$ in the absence of particle production. In fact the density changes by a large factor within the mean free path of the particles. A fluid description of the plasma, although perhaps useful for roughly estimating its behavior, is not self-consistent.

*Present address: McGill University, Montréal, Québec, Canada H3A 2T8 and Service de physique théorique du CEA Saclay, F-91191 Gif-sur-Yvette cédex, France.

It thus seems worthwhile to investigate the evolution of the Hawking radiation plasma more quantitatively. The proper framework for doing so is the Boltzmann equation for the particle distributions,

$$\left(\frac{\partial}{\partial t}+\frac{\mathbf{p}}{E}\cdot\boldsymbol{\nabla}\right)f(\mathbf{p},\mathbf{x},t)=\mathcal{C}[f(\mathbf{p},\mathbf{x},t)] \tag{2}$$

using Eq. (1) as a boundary condition at $r=r_H$. In the following section we will discuss a general method for solving the Boltzmann equation which has been successfully used in the field of heavy ion collisions, and the adaptations of this method which we have made for the BH problem. Crucial for this investigation is the collision term $\mathcal{C}[f]$. Section III focuses on the scattering cross sections which go into $\mathcal{C}$. In Sec. IV we present our results for the detailed properties of the QED and QCD photospheres. The ramifications for the most relevant observable particle backgrounds, namely gamma rays and antiprotons, are worked out in Sec. V. We summarize our results in the final section.

II. TEST PARTICLE METHOD FOR SOLVING BOLTZMANN EQUATION

The full Boltzmann equation is an integro-differential equation which is difficult to solve exactly. For black holes we can make several important simplifications. (1) We consider nonrotating black holes so that the distribution functions have spherical symmetry. (2) We confine our attention to BH's whose lifetime is still long compared to the diffusion time of particles in the putative photosphere; thus the distribution functions are approximately time-independent. For example, the lifetime of a black hole with $M=10^{11}$ g and $T=1000$ GeV is of order 10^5 s, whereas the particle diffusion time in its photosphere is $\sim 10^{-21}$ s. We estimate that only for black holes of mass $\lesssim 10^7$ g will the lifetime become comparable to the diffusion time.

Under the above assumptions, the Boltzmann equation takes the simpler form

$$\frac{\partial}{\partial r}f(p,p_t,r)=\frac{1}{v_r}\mathcal{C}[f], \tag{3}$$

where $p=|\mathbf{p}|$, p_t is the magnitude of the component of momentum transverse to the radial direction, and v_r is the radial velocity. Because of the spherical symmetry there is no dependence on the azimuthal momentum component.

Even with these simplifications, Eq. (3) is still prohibitively difficult to solve in the most naive numerical way, namely discretizing momentum space and evolving the distribution defined on this momentum lattice forward in radius. At each point in momentum space a multidimensional phase space integral is required to evaluate the collision term, which is computationally costly. Fortunately, this problem has been already surmounted in other situations, namely heavy ion collisions [11,12]. There one wants to track the distribution functions of nucleons in the two nuclei as they pass through each other and undergo collisions.

The idea is essentially to follow the classical evolution of each particle, allowing for possible scatterings by using the differential scattering cross section as a probability distribution. However, the number of nucleons in even a heavy nucleus is so small that one must do this many times to obtain distribution functions that are not dominated by statistical fluctuations. Alternatively, one can obtain the required statistics by representing each real particle by an arbitrarily large number of test particles, which is equivalent to but simpler than simulating the heavy ion collision many times. One must only be sure to avoid unphysical collisions by prohibiting any two test particles that represent the same actual particle from scattering off each other. However, in practice, it is easier to allow scatterings to occur between *all* test particles, while simultaneously reducing the cross section by a factor N, equal to the ratio between the number of test particles and the number of actual particles.

A difference between heavy ion collisions and black hole radiation is that in the former, one is evolving the distributions in time, whereas we want to evolve them in space. However, our version of the Boltzmann equation is mathematically equivalent to one with time evolution but spatial homogeneity,

$$\frac{\partial}{\partial t}f(\mathbf{p},t)=\mathcal{C}'[f], \tag{4}$$

where $f(\mathbf{p},t)$ is known at some initial time. Since this equation is evidently amenable to solution by the test particle method, and Eq. (3) is equivalent to it just by renaming $t\to r$ and $\mathcal{C}'[f]\to\mathcal{C}[f]/v_r$, we can also apply the same method to solve Eq. (3).

A. Free evolution

Let us first consider how the method works in the absence of collisions, so the particles are propagating freely. At the initial surface of the horizon, it is assumed that the radiation is distributed according to Eq. (1) in all directions not pointing back below the horizon, that is, for polar angles with $\cos\theta>0$. However, at a larger radius r, if there have been no collisions then particles can only have come from a cone pointing back to and subtended by the horizon. The directions of the possible momenta of the particles are restricted to lie in the outward half of this cone, whose opening angle is given by $\sin\theta=r_H/r$. As r increases, the momenta become increasingly concentrated in the radial direction.

Numerically the evolution in the noninteracting case is thus trivial. A particle whose momentum is $\mathbf{p}$ at r_H will have the same momentum at $r'>r$. However, the *coordinates* of the momenta will change: for example, if $\mathbf{p}$ is purely transverse at r, it will develop a radial component at r'. Let θ be the polar angle from the radial direction at r and θ' that at r' (see Fig. 1). Then using the law of sines,

$$\sin\theta'=\frac{r}{r'}\sin\theta. \tag{5}$$

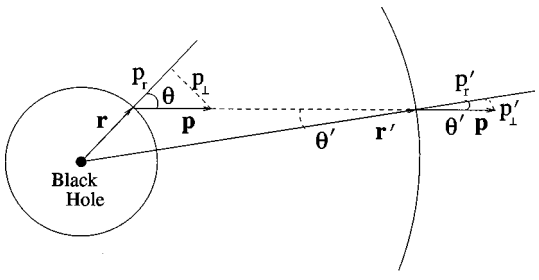

FIG. 1. Momentum in free radial evolution.

For very large r' the momentum becomes essentially radial, $\theta' \cong 0$, and a momentum that is initially radial remains so. The distribution function will be given approximately by

$$f(\mathbf{p}',r') \cong \begin{cases} f(\mathbf{p},r_H), & 0 \leqslant \sin\theta' \leqslant r_H/r, \\ 0, & \sin\theta' > r_H/r, \end{cases} \tag{6}$$

where the new radial and perpendicular components are related to the old ones by

$$p'_\perp = \frac{r_H}{r} p_\perp \quad \text{and} \quad p'_r = \sqrt{p^2 - p'^2_\perp}. \tag{7}$$

If f is isotropic at the horizon, then for large distances one finds that this gives a density decreasing like $1/r^2$, as required by conservation of particle flux:

$$n(r) = \int \frac{d^3p}{(2\pi)^3} f(\mathbf{p},r) = \left(\frac{r_H}{r}\right)^2 n(r_H). \tag{8}$$

Since the particles are moving on straight lines, the step size for evolving the distributions is irrelevant in the noninteracting case.

B. Including interactions

To account for the interactions of the particles with each other one must first choose an appropriate step size Δr for evolving the distribution. The natural choice is the mean free path, λ, or some fraction thereof. If the interaction cross section is σ, then we can define

$$\lambda^{-1}(r) = n(r)\langle \sigma v_{rel} \rangle, \tag{9}$$

where n is the density and v_{rel} is the relative velocity of the two interacting particles (to be discussed in more detail below, in Sec. III). However, the time-independent Boltzmann equation we are solving is mathematically equivalent to the usual time-dependent version only after dividing by the radial velocity. Thus our collision term is related to the usual one by a factor of $1/v_r$, which modifies the definition of the mean free path to

$$\lambda^{-1}(r) = n(r)\left\langle \sigma \frac{v_{rel}}{v_r} \right\rangle. \tag{10}$$

We take v_r in this formula to be the minimum of the radial velocities of the two interacting particles. In practice this factor is not very important because the bulk flow of the particles away from the black hole tends to cause v_r to approach unity.

The average is taken using the distribution functions for the incoming particles,

$$\left\langle \sigma \frac{v_{rel}}{v_r} \right\rangle = \int \frac{d^3p_1 d^3p_2}{(2\pi)^6} f(\mathbf{p_1},r) f(\mathbf{p_2},r) \sigma \frac{v_{rel}}{v_r}. \tag{11}$$

In the test particle method, there is no need to do any integrals *per se*. Since the ensemble of test particles is already distributed according to f, $\langle \sigma v_{rel}/v_r \rangle$ is simply given by an unweighted average of $\sigma v_{rel}/v_r$ over the ensemble. We randomly choose pairs of particles to perform this average.

If $\lambda(r)$ was constant, one could choose the step size for the evolution to be simply $\Delta r = \lambda$. Since λ is the average distance particles go between collisions, the interactions could be simulated by demanding that over the distance $\Delta r = \lambda$, each particle participates in a single collision. However, in the black hole problem $\lambda(r)$ can increase significantly on a distance scale of λ because the density is decreasing like $1/r^2$. To deal with this, one must choose the step size to be smaller,

$$\Delta r \ll \frac{\lambda}{d\lambda/dr}. \tag{12}$$

Then λ, and hence the interaction rate, is guaranteed to be approximately constant over Δr. Over this distance, only a fraction F of all the particles will undergo scattering,

$$F = \frac{\Delta r}{\lambda}. \tag{13}$$

The general procedure for including interactions is therefore clear: (1) At each r, compute λ using the known distributions $f(\mathbf{p},r)$. (2) Given λ, choose a step size Δr in accordance with Eq. (12). (3) Choose a subset of particles from the ensemble such that a fraction $F = \Delta r/\lambda$ of the total ensemble will undergo collisions and change their energies and momenta accordingly. To account for the $1/v_r$ factor in the effective cross section, we arrange the ensemble in order of increasing v_r and let that fraction of particles F with the smallest v_r participate in the interactions. After these steps are carried out, the distribution function is known at $r + \Delta r$ and the procedure can be repeated.

The particle density $n(r)$ which goes into Eq. (10) is calculated analytically and therefore does not depend on the number of the test particles. To find the density $n(r)$ we first compute what it would be in the absence of particle production:

$$n_0(r) = n_h \frac{r_h^2}{r^2}, \tag{14}$$

where the subscript 0 means that this density is before the particle creation process is taken into account. The radius of the horizon is $r_h = 1/(4\pi T_{BH})$. To find the density at the horizon, we note that if the BH absorption cross section

$\sigma(E)$ was a constant, then the BH would be a perfect black body, and the density of radiation would be thermal. However $\sigma(E)$ is suppressed as $E\to 0$ and only reaches its geometric optics value of $\sigma_0=27\pi G^2M^2$ in the limit as $E\to\infty$. Therefore n_h is reduced from its thermal value by a factor of $\Gamma_s\equiv\int d^3p\,\sigma(E)f_\pm(p)/\int d^3p\,\sigma_0 f_\pm(p)$. This has been computed in Ref. [8] to be

$$\Gamma_s=\begin{cases}\dfrac{56.7}{27\pi} & \text{electrons,}\\[2ex] \dfrac{20.4}{27\pi} & \text{photons.}\end{cases} \tag{15}$$

Then the density at the horizon is

$$n_h=\begin{cases}\dfrac{3}{2\pi^2}\Gamma_f\zeta(3)T_{BH}^3 & \text{electrons or positrons,}\\[2ex] \dfrac{2}{\pi^2}\Gamma_b\zeta(3)T_{BH}^3 & \text{photons,}\end{cases} \tag{16}$$

where $\zeta(3)=1.20206$ (Rieman zeta function).

To account for particle creation we use the test particles to find the fraction of new fermions and bosons created at each step. Let $N_{f[b]}(r)$ be the number of electrons [photons] in the shell of width Δr at radius r. We will define $P_{f[b]}(r)$ as

$$P_{f[b]}(r)=\frac{N_{f[b]}(r)}{N_{f[b]}(r_h)}. \tag{17}$$

Then, using Eq. (14) through (17) we obtain

$$n(r)=\frac{\zeta(3)}{\pi^2(4\pi)^2}\frac{T_{BH}}{r^2}\begin{cases}\dfrac{3}{2}\Gamma_f P_f(r), & e^+ \text{ or } e^-\\[2ex] 2\Gamma_b P_b(r), & \gamma.\end{cases} \tag{18}$$

In this way, particle densities can be computed at any step by keeping track of the relative increase in particle number, $P_{f[b]}$. Later, we shall also refer to the ratio of all particles at r versus at the horizon;

$$P(r)=\frac{n_b(r)+n_f(r)}{n_b(r_h)+n_f(r_h)}=\frac{P_b(r)+4.17P_f(r)}{1+4.17}. \tag{19}$$

The factor 4.17 comes from computing $3\Gamma_f/2\Gamma_b$.

To generalize the previous results to quarks and gluons is straightforward: one must multiply the photon density by a factor of 8 to convert to gluons, and the electron density by a factor $3n_f$ to get n_f flavors of quarks.

A final issue concerns the number of test particles used to represent the ensemble, versus the actual number of particles coming from the BH. For example, within the first radial increment Δr near the horizon, the actual number of particles $\Delta N=4\pi r_H^2\Delta r n(r_H)$ might be too small a number to generate a smooth distribution function. We would prefer to represent these particles with some much larger number N_t of test particles. In the application to heavy ion collisions it is necessary to reduce the cross section by the factor $\Delta N/N_t$ to avoid overestimating the number of collisions. This is because in the latter situation, individual nucleon positions are kept track of, and two particles are only allowed to collide if they come within a distance $b_c=\sqrt{\sigma/\pi}$ of each other. If the number of particles is artificially increased while proportionally decreasing the cross section, the physically meaningful mean free path will remain constant. In our case, since we do not follow the spatial trajectories of particles, but instead compute the physical mean free path, it is consistent to allow *all* the test particles to interact over a distance λ, regardless of how large the ratio $N_t/\Delta N$ is. Thus there is no need to reduce σ proportionally to the number of test particles in the present problem.

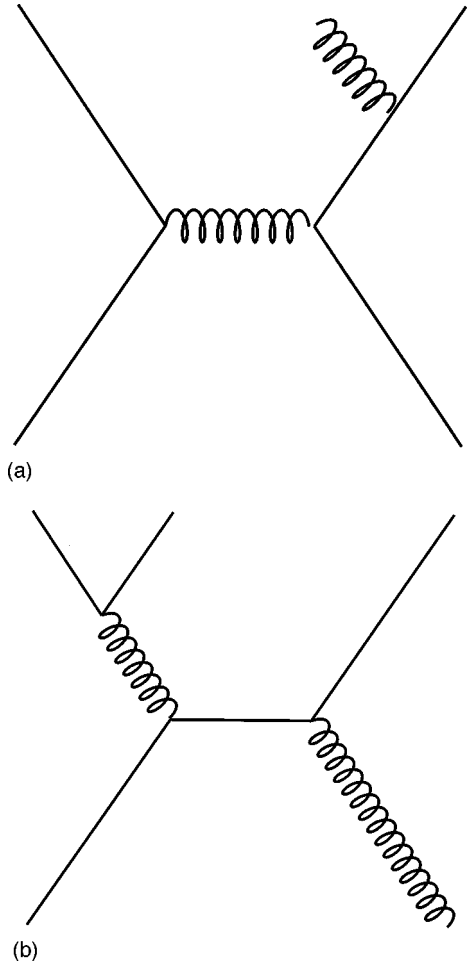

FIG. 2. Feynman diagrams for the dominant contributions to (a) bremsstrahlung; (b) pair production.

III. SCATTERING CROSS SECTION

The most important processes contributing to photosphere formation around the BH are bremsstrahlung ($ee\to ee\gamma$) and photon-electron pair production ($e\gamma\to ee^-e^+$), whose dominant Feynman diagrams are shown in Fig. 2. Both have cross sections of $O(\alpha^3)$, which at first sight might make

them seem less important than the leading $O(\alpha^2)$ processes like Compton scattering. However the latter are elastic and change the distributions only by randomizing the momenta, whereas the former are inelastic and increase the number of particles while reducing their average energies. Thus the elastic scattering processes appear to be less relevant for determining the properties of the photosphere even though they are faster than the inelastic ones. Before going on to a detailed description of bremsstrahlung, let us examine this issue more carefully.

A. Elastic scattering processes

One could argue that elastic interactions like Compton scattering ($e\gamma \to e\gamma$) or electron-electron scattering might change the size of the photosphere somewhat, but they will not affect the most important observable property, which is the energy spectrum of emitted particles. It is the $2 \to 3$ body interactions like bremsstrahlung which principally distinguish the photosphere from freely streaming particles. However there is one sense in which elastic scatterings may be important: by randomizing the particle momenta, they might postpone the tendency for the relative velocities of particles to approach zero, due to the bulk, outward radial motion. This in turn could keep the bremsstrahlung mean free path, Eq. (10), small out to larger radii, enlarging the size of the photosphere.

Suppose the mean free path for elastic processes is given by $\lambda_e(r)$ at a distance r from the black hole. Their momentum-randomizing effects will be important for the photosphere only in regions where $\lambda_e \lesssim r$. This is because the length scale over which random momenta become increasingly radial at a given distance r is r itself. If $\lambda_e(r)$ exceeds r, then scatterings start to lose in the competition against geometry.

The relativistic limit of the Compton cross section, in the laboratory frame, is

$$\sigma_c = \frac{2\pi\alpha^2}{m_e E} \ln \frac{E}{m_e}. \tag{20}$$

We can then estimate λ_e as

$$\lambda_e^{-1}(r) \cong \sigma_c n(r) = \sigma_c n(r_h) P(r), \tag{21}$$

with the particle density given by Eq. (18) and the particle production factor by Eq. (19). Below, we will show that when elastic scattering is ignored, the QED photosphere ends at a distance of $r_f \sim m_e^{-1}$, and for large T_{BH}, $P(r_f) \sim b T_{BH}^2$ with $b = 4.5 \times 10^{-5}\ \mathrm{GeV}^{-2}$. Furthermore, the average particle energy at the horizon will be given by its value at the horizon, $\sim 3T_{BH}$, divided by $P(r)$. To see whether our neglect of elastic scattering is consistent, we should compute $r_f/\lambda_c \cong (m_e \lambda_c)^{-1}$, and ask whether it ever exceeds $O(1)$. Using the above results we get

$$\frac{1}{m_e \lambda_c} \cong \frac{\sigma_c}{m_e}\left(n(r_h) \frac{r_h^2}{r_f^2} P(r_f) \right) = 4.3 \left(\frac{T_{BH}}{10\ \mathrm{TeV}} \right)^4 \left(9.5 - \ln\left(\frac{T_{BH}}{10\ \mathrm{TeV}} \right) \right). \tag{22}$$

Therefore the effects of elastic scattering should only become important when the BH temperature starts to exceed ~ 5 TeV. We will discuss our numerical investigation of this regime below, although most of our work focuses on BH temperatures below 1 TeV.

B. Bremsstrahlung cross section

The relativistic differential cross section for bremsstrahlung in the center of mass frame is [13,14]

$$\frac{d\sigma(\omega)}{d\omega} \approx \frac{8\alpha r_e^2}{E\omega}\left(\frac{4}{3}(E-\omega) + \frac{\omega^2}{E} \right)\left(\ln\left[\frac{4E^2(E-\omega)}{m_e^2 \omega} \right] - \frac{1}{2} \right), \tag{23}$$

where $\hbar = c = 1$, $r_e = \alpha/m_e$, E is the initial energy of each electron, and ω is the energy of the emitted photon. It diverges for $\omega \to 0$, but higher order corrections essentially impose an infrared cutoff [7].

The form of Eq. (23) implies that the probability to emit a photon diverges as its energy goes to zero. On the other hand, emission of a zero-energy photon has no effect on the electron which emits it. A convenient way of rendering the cross section finite, while at the same time accounting for the photons which carry away significant energy, is to use the energy-averaged total cross section [7,13]

$$\overline{\sigma} = \int \frac{\omega}{E}\left(\frac{d\sigma}{d\omega} \right) d\omega \approx 8\alpha r_e^2 \ln \frac{2E}{m_e}. \tag{24}$$

The cross section for photon-electron pair production shows the same functional dependence in the extreme relativistic limit and we therefore use the same estimate (24) for both interactions.

An improvement on the present treatment would be to use the actual differential bremsstrahlung cross section as a distribution which would produce low energy photons with higher probability. One would have to impose an infrared cutoff on the emitted photon energy and show that no meaningful physical properties of the photosphere depend on this cutoff. Here we have taken the simpler approach of approximating $d\sigma/d\Omega = \overline{\sigma}/4\pi$, and choosing the energies and directions of the final state particles at random in the center of mass system, subject to the constraint of conservation of four-momentum.

C. Thermal mass

Bremsstrahlung processes do not occur in vacuum but in a background plasma of almost radially propagating particles. These background particles suppress the bremsstrahlung cross section if they are sufficiently dense (the LPM effect [20]). A simplified means of accounting for this is to replace the vacuum electron mass, m_e, by its thermal value,

$$m_{th}=\sqrt{m_e^2+m_p^2(T)}. \tag{25}$$

This procedure, although not exact, gives the correct position of the pole of the electron propagator in the energy-momentum plane to an accuracy of 10% [15]. In a gauge theory with coupling constant g, in a thermal background, the plasma mass is given by $m_p=gT\sqrt{C(R)/8}$, where $C(R)$ is the quadratic Casimir invariant for the fermion transforming in the representation R of the gauge group. However, even if the background is not in thermal equilibrium, we find by computing the electron self-energy in the plasma that the formula for m_p which was originally derived in the thermal case is still correct:

$$m_p^2=g^2C(R)\int\frac{d^3p}{(2\pi)^3p}(f_f(p)+f_b(p)), \tag{26}$$

where $f_{f(b)}(p)$ is the distribution function for a single polarization of the background fermions (gauge bosons), [i.e., $f_{f(b)}(p)=(e^{E/T}\pm 1)^{-1}$ in the thermal case]. For a collection of test particles which represents these distribution functions, the integral may be approximated by taking the average of $1/p$ over all electrons and photons, respectively (quarks and gluons in the case of QCD). Counting polarizations, we obtain

$$m_p^2\simeq\begin{cases}4\pi\alpha(n_e\langle p_e^{-1}\rangle+n_\gamma\langle p_\gamma^{-1}\rangle), & \text{QED}\\ \dfrac{16\pi}{3}\alpha_s\left(\dfrac{n_q}{3n_f}\langle p_q^{-1}\rangle+\dfrac{n_g}{8}\langle p_g^{-1}\rangle\right), & \text{QCD.}\end{cases} \tag{27}$$

Near the BH horizon where the particle densities are high, the plasma mass dominates over the vacuum mass, and leads to a significant reduction in the bremsstrahlung cross section, since $\overline{\sigma}\propto m_{th}^{-2}$. Failure to take this into account would give a misleading estimate of the onset of the photosphere in the case of QED.

Several aspects of the implementation of thermal mass in the test particle model should be mentioned. First, in Eq. (27) n_e and n_γ are the actual electron and photon densities calculated analytically, whereas p_e and p_γ are kinetic energies of the test particles, assumed to be relativistic. Secondly, we recalculate the fermion thermal mass [using Eq. (25)] at each step in radius. Because m_{th} changes, if the fermion momentum was held fixed, its total energy $E=\sqrt{m_{th}^2+p_e^2}$, would change. Hence, we assume that the thermal mass correction is done at the expense of momentum in such a way as to keep its total energy E constant.

[The reader may wonder whether energy should indeed be conserved, due to gravitational redshift. In fact all significant redshifting of the outgoing particle energies occurs within the first few Schwarzschild radii of the horizon, where the classical concept of particles is not yet well defined, due in part to the de Broglie wavelength being of the same order as the Schwarzschild radius. Moreover, the Hawking spectrum (1) refers to energies as observed far from the BH. If we were going to try to include redshift effects, we should blueshift the initial particle energies accordingly, so that asymptotically they have the usual distribution. This would only affect our simulation very close to the horizon, which does not appear to be an important region as regards the observable features of the photosphere. Hence it is simpler and seemingly a good approximation to ignore redshift.]

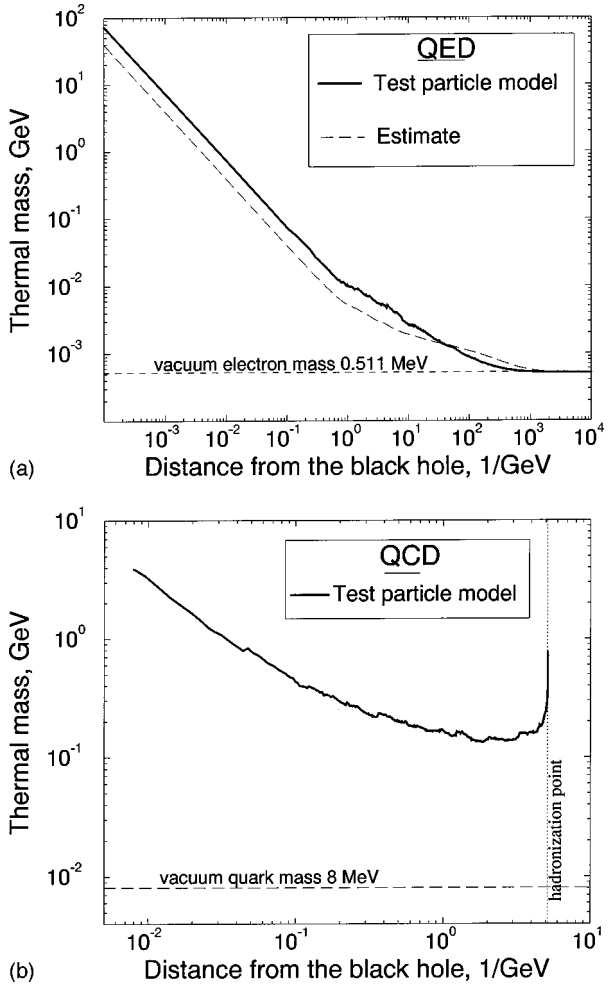

FIG. 3. Thermal mass [and the estimate (28)] in typical (a) QED and (b) QCD photospheres.

As in Ref. [7], we can estimate the thermal mass of an electron in the QED photosphere using $n(r)=T_{BH}(3/2)^{\mathcal{N}(r)}/(\pi^2(4\pi)^2r^2)$ for the densities of both photons and electrons, and $3T_{BH}/(3/2)^{\mathcal{N}(r)}$ for average particle energy at radius r. Here, $\mathcal{N}(r)$ is the number of bremsstrahlung events an average particle undergoes between the horizon and radius r. Since in each such scattering one new particle is produced, $(3/2)^{\mathcal{N}(r)}$ is the factor by which the total number of particles has increased. In the test-particle model, since the total number of particles $N(r)$ is known at each step, this increase is calculated directly as $N(r)/N(r_h)$. Then,

$$m_{th}\simeq\sqrt{m_e^2+\frac{\alpha}{\pi(4\pi)^2}\frac{1}{r^2}\left(\frac{N(r)}{N(r_h)}\right)^2}. \tag{28}$$

Figure 3 shows how the thermal mass depends on radial distance from the BH for two illustrative cases: the QED photosphere of a BH with $T=1000\,\mathrm{GeV}$, and the QCD

photosphere for a $T=10\,\mathrm{GeV}$ black hole. We see that in the QED plasma the factor of $1/r^2$ is dominant over any growth in density as the radius increases, which causes the thermal mass to decrease monotonically. On the other hand, in the QCD plasma, the particle production factor $N(r)/N(r_h)$ is more influential (due to the running of the coupling constant with energy, in particular) and just before hadronization starts, at average particle energies $\langle E\rangle$ near the QCD scale Λ_{QCD}, the thermal mass may again increase. Our perturbative formulas should not be trusted quantitatively in this regime, however. Figure 3(a) also shows that the analytic approximation (28) m_{th} and the numerically computed values are in reasonably good agreement.

D. Interaction distance and relative velocity

The distance at which particles can interact via bremsstrahlung and pair production is an important parameter, since we have to decide which test particles may interact with one another and which may not. In the heavy ion collision problem, those test particles were allowed to interact which were within a critical distance $b_c=\sqrt{\sigma/\pi}$ from each other. Notice that in that case, the relative velocity of the two particles was typically large because the interacting nucleons were not moving parallel to each other. But in the present case of BH radiation, two particles which are nearest neighbors typically are moving in almost the same direction, i.e., radially, leading to a suppressed relative velocity v_{rel}. Such particles have a small probability of interacting, since they make a small contribution to the inverse mean free path, Eq. (9). The dominant interactions involve pairs of particles with large relative velocity. Near the horizon of the BH, such pairs would consist of particles on opposite sides of the BH, moving away from each other.

Although classically it is somewhat counterintuitive to have interactions between particles that have already passed each other, as it were, there is no reason to exclude them so long as the particles are still within the range of the interaction. For bremsstrahlung it has been shown [16] that at relativistic energies, small momentum transfers of the order $k\simeq m_e$ contribute the bulk of the total cross section. Therefore the distance at which particles can interact via bremsstrahlung (and pair production) is of order m_e^{-1} in the vacuum. In the plasma, accounting for the LPM effect, the cutoff instead becomes the thermal mass m_{th}^{-1}.

Therefore in the radial interval $r_h<r<m_{th}^{-1}$ (assuming the BH is microscopic so that the photosphere can indeed form), a given particle in the plasma is always able to interact with some other particle, with a large relative velocity, $v_{rel}\lesssim 2$. It is not necessary to assume particles interact only with their nearest neighbors, or to keep track of the exact spatial trajectories of the particles, which simplifies our task of evolving the ensemble of test particles.

Of course the above procedure no longer works at radii larger than m_{th}^{-1}. At that point we adopt the procedure of randomly pairing particles, assuming the pairs represent nearest neighbors separated by the average interparticle distance $n(r)^{-1/3}$, and computing their actual relative velocity, given by the formula

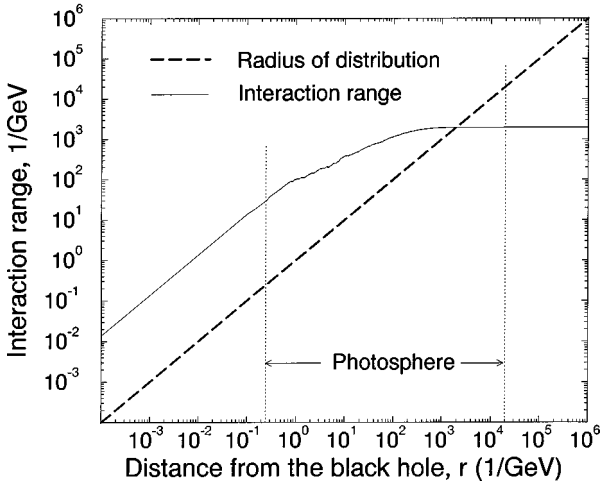

FIG. 4. Maximum distance of interaction, m_{th}^{-1}, in a typical QED photosphere ($T_{BH}=1000\,\mathrm{GeV}$), indicating the rapid dissipation of the photosphere at distances $r>m_{th}^{-1}$.

$$v_{rel}=\frac{\sqrt{(p_1\cdot p_2)^2-m_1^2m_2^2}}{E_1E_2}$$

$$\cong\sqrt{2\left(1-\frac{\mathbf{p_1}\cdot\mathbf{p_2}}{p_1p_2}\right)}, \tag{29}$$

whose second form is valid in the relativistic limit.[1] In this large-radius regime we rely upon the randomization of velocities provided by the scatterings themselves to keep the momenta from becoming purely radial, which otherwise causes v_{rel} to tend toward zero. Nevertheless the inevitable radialization of momenta as r increases quickly overcomes the randomization due to scatterings, causing the particles to become freely propagating and marking the end of the photosphere. This behavior is shown in Fig. 4. Although our matching between the $r<m_{th}^{-1}$ and $r>m_{th}^{-1}$ regions is somewhat crude, we believe it captures the essential physics, and that a more accurate treatment, using detailed information about each particle's trajectory, would only change the estimate of the photosphere's outer radius by a factor of order unity.

IV. NUMERICAL RESULTS: QED PHOTOSPHERE

This section will summarize the results of test particle simulation of black hole emission when only electrons, positrons and photons are taken into consideration. This restriction is appropriate for black holes with $T_{BH}<\Lambda_{QCD}$. We will also treat higher temperatures in this context for the sake

[1]This definition of v_{rel} arises from comparing the detailed form of the collision term in the Boltzmann equation with that of the scattering cross section. It is important to notice that the scattering angle between $\mathbf{p}_1$ and $\mathbf{p}_2$ is evaluated in the rest frame of the BH. This is the same frame in which the Boltzmann equation is most naturally formulated for the present problem.

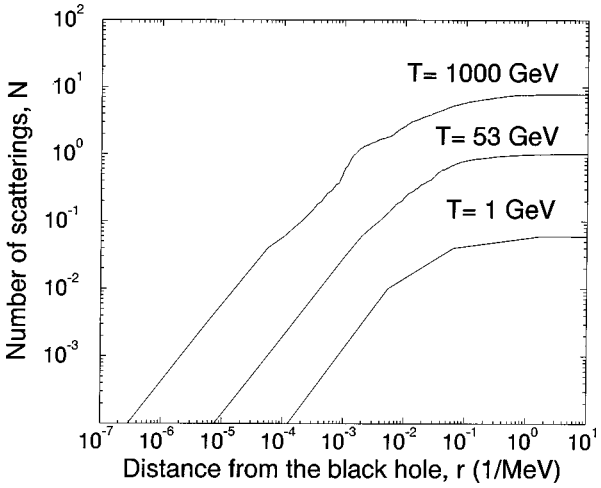

FIG. 5. The number of scatterings an average particle undergoes between the horizon and radius r: $\mathcal{N}(r)$.

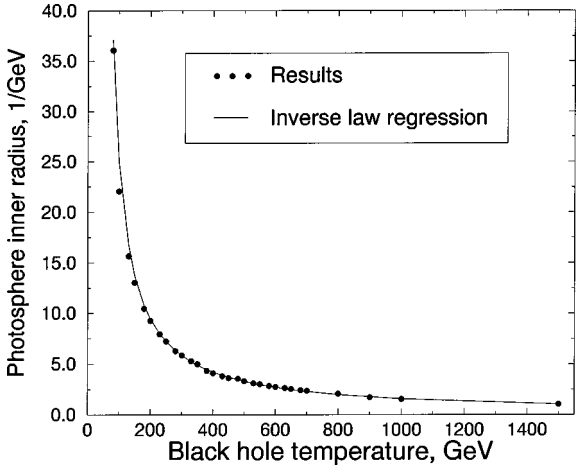

FIG. 6. Radii of inner QED photosphere surface for different black hole temperatures (black dots). Solid line represents inverse regression over these values; see Eq. (31).

of understanding, deferring study of the effects of quarks and gluons until the next subsection.

A. Photosphere formation

We confirm the formation of a photosphere for black hole temperatures $T_{BH}\sim 100\,\mathrm{GeV}$ and higher, as was originally suggested in [7]. The photosphere first appears at a radius $r_0\sim 10^4 r_h$ (where $r_h=1/4\pi T_{BH}$ is the Schwarzschild radius), and is characterized by a region of intense collisions terminating at a distance of $r_f\sim 10^7-10^8 r_h$ from the black hole. The effectiveness of the collisions is demonstrated by a very slow increase, or even decrease, of the mean free path in the photosphere compared to the interior and exterior regions.

The photosphere forms only for black holes above a certain critical temperature T_c. We use the same definition of T_c as was introduced by Heckler [7]. The idea is to define a quantity $\mathcal{N}(r)$ denoting the number of scatterings an average particle undergoes between the horizon and some radius $r>r_h$. The criterion for having a photosphere is taken to be that on average every particle undergoes a collision at least once between leaving the horizon and escaping to infinity, in other words that

$$\lim_{r\to\infty}\mathcal{N}(r)\geqslant 1. \tag{30}$$

T_c is then the temperature of a black hole for which this limit is exactly unity. The critical temperature we obtain is $T_c\simeq 50\,\mathrm{GeV}$, whereas the result following from the approximate method of Ref. [7] is 45.2 GeV. Our determination of $\mathcal{N}(r)$ is shown for several black hole temperatures in Fig. 5.

B. Photosphere parameters

Here we will present the photosphere parameters obtained from simulations for approximately 30 different black hole temperatures. These parameters include the radii of the inner and outer surfaces, r_i and r_f respectively, the total particle production factor P and the average energy of the particles emerging from the photosphere $\overline{E_f}$. The latter is relevant because it is the average energy of particles that may eventually reach a distant observer. We will point out significant discrepancies between these results and the fluid model used in [7], and derive empirical formulas from our simulations showing the dependence of r_i, r_f and $\overline{E_f}$ on the BH temperature, T_{BH}.

Inner radius

The radius of the inner surface of the photosphere (r_i) is defined by $\mathcal{N}(r_i)=1$, i.e., the radius by which on average every particle originating at the horizon has undergone one collision. The values of r_i in units of $1\,\mathrm{GeV}^{-1}\simeq 0.197$ fm are plotted in Fig. 6 as a function of black hole temperature. As one can see from the graph, r_i decreases with the temperature and is closely fitted by

$$r_i=\frac{1}{\kappa T_{BH}},\quad \kappa=(6.446\pm 0.003)\times 10^{-4}. \tag{31}$$

We know that the radius of the Schwarzschild horizon is also inversely proportional to the black hole temperature $r_h=1/4\pi T_{BH}$, so that

$$r_i=\frac{4\pi}{\kappa}r_h\simeq 2\times 10^4 r_h. \tag{32}$$

By this criterion, the photosphere starts to develop much closer to the black hole than was predicted ($r_i\sim 10^9 r_h$) in [7] using a fluid model for the interacting particles.

Edge radius

The outer radius of the photosphere, r_f, can be defined as the distance after which particles effectively free stream away without significant interactions with one another. The mean free path λ quickly begins to diverge at this point. If λ_i is the mean free path at step i then the condition λ_{i+1}/λ_i

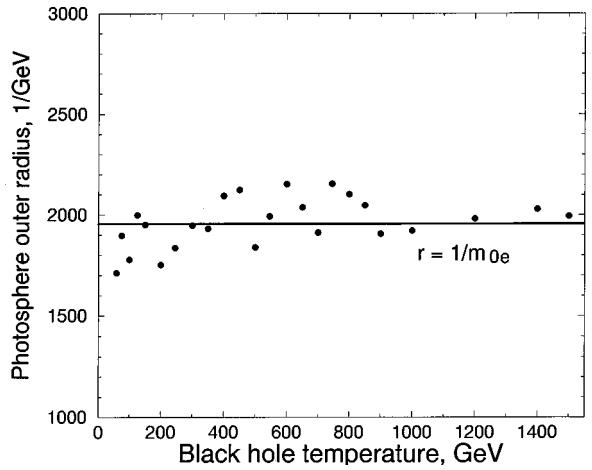

FIG. 7. Radii of outer QED photosphere surface for different black hole temperatures. The solid line shows $r=1/m_e$, the radius beyond which particles can no longer interact with each other by bremsstrahlung.

$\gg\lambda_i/\lambda_{i-1}$ is a convenient criterion to define the end of the photosphere, and r_f is just the radius the particles have reached by step i. This value is easily found in practice because in the next step after r_f, λ is usually several orders of magnitude larger than its previous value, implying that the particles have become virtually free. Because $\lambda(r)$ is diverging so quickly near r_f, the latter is inherently difficult to determine precisely, even when the steps size is made smaller near the edge of the photosphere. Great precision in r_f is not essential, however, because it is not an observable quantity.

The values of r_f remain in the same range $(1700-2200\,\mathrm{GeV}^{-1})$ for all black hole temperatures shown and are consistent with being independent of T_{BH} at the horizon. Only the statistical dispersion around the mean value decreases with rising temperature (Fig. 7). The mean value is approximately $r_f\sim 2000\,\mathrm{GeV}^{-1}$, which is close to $1/m_e$. This is easy to understand in light of our previous discussion (Sec. III C and Fig. 3) of the range of the bremsstrahlung interaction, whose maximum value is of order $1/m_e$. Because the trajectories of particles within the range of interaction rapidly become parallel at radii beyond this cutoff, the photosphere quickly dissipates.

Particle production

Another useful parameter for characterizing the photosphere is the total particle production factor, given by $P=N(r_f)/N(r_h)$, where $N(r)$ is the number of test particles at radius r. P can be used to quantify the probability of interactions inside the photosphere, since at each collision $N\rightarrow N+1$. Figure 8 shows P as a function of black hole temperature. We find that it can be represented by a quadratic fit (solid line):

$$P(T_{BH})\simeq aT_{BH}+bT_{BH}^2, \tag{33}$$

where

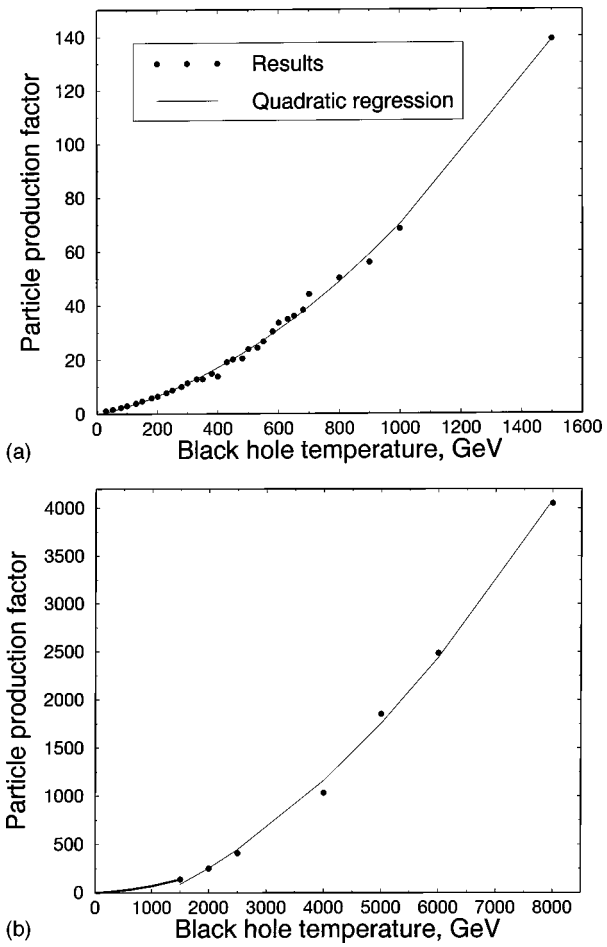

FIG. 8. Particle production factor $N(r_f)/N(r_h)$ versus T_{BH} for (a) $T_{BH}<1.5$ TeV and (b) $T_{BH}<8$ TeV. Solid line is the quadratic fit to the results [Eq. (33)].

$$a=\begin{cases}0.026\ \mathrm{GeV}^{-1}, & T_{BH}<2\ \mathrm{TeV};\\ 0.226\ \mathrm{GeV}^{-1}, & T_{BH}>2\ \mathrm{TeV};\end{cases}$$

$$b=\begin{cases}4.5\times10^{-5}\ \mathrm{GeV}^{-2}, & T_{BH}<2\ \mathrm{TeV};\\ 4.2\times10^{-5}\ \mathrm{GeV}^{-2}, & T_{BH}>2\ \mathrm{TeV}.\end{cases} \tag{34}$$

The dominant quadratic term implies that the particle number density in the photosphere increases rapidly in the last stages of black hole evaporation, as T approaches the Planck scale. The slightly different dependences for $T_{BH}>2$ TeV and $T_{BH}<2$ TeV can be understood by the argument of Sec. III A: this is the temperature where randomizing effects of elastic scattering become relevant. However, the effect is not dramatic.

Average final energy

From an observational point of view, the reduction in average energy of emitted particles is one of the most relevant consequences of the photosphere. At the horizon, $\overline{E_i}$ is approximately $3.1T_{BH}$. But the photosphere can reduce this number dramatically, so that a distant observer sees a much softer spectrum. Our results for the T_{BH} dependence of the

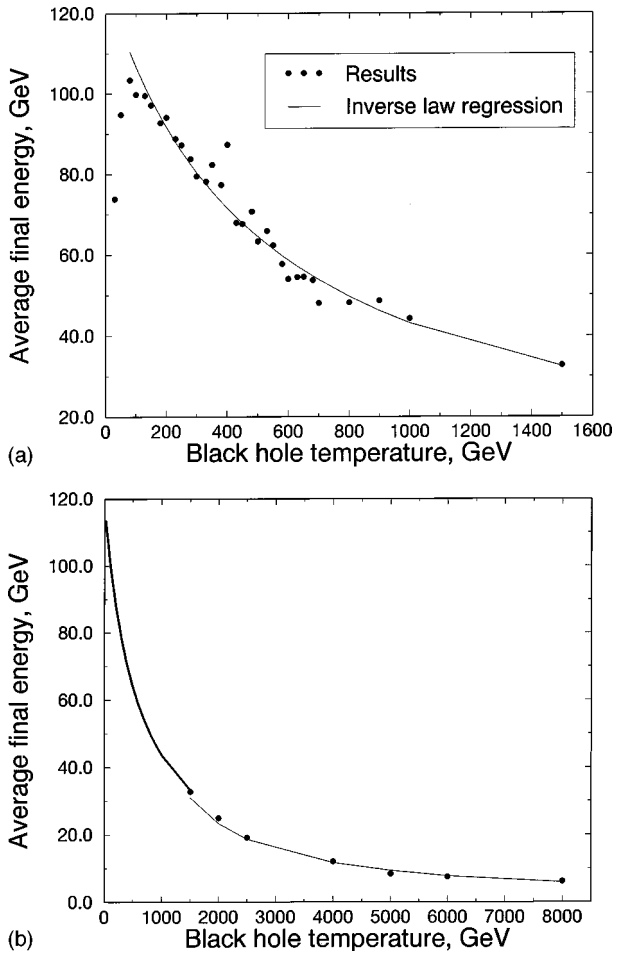

FIG. 9. $\overline{E_f}$, average particle energy at the outer edge of the QED photosphere, for (a) $T_{BH}<1.5$ TeV and (b) $T_{BH}<8$ TeV.

average energy at the edge of the photosphere, $\overline{E_f}$, are displayed in Fig. 9. These values are significantly higher than those (~ 1 MeV) found in Ref. [7], and the temperature-dependence is also very different. This apparently stems from the use of a fluid description in [7] which is not really applicable.

We can compute $\overline{E_f}$ from $\overline{E_i}$ and the particle production factor, Eq. (33):

$$\overline{E_f}=\frac{\overline{E_i}}{P}=\frac{\left(2.7\frac{n_b}{n}+3.15\frac{n_f}{n}\right)T_{BH}}{aT_{BH}+bT_{BH}^2}$$

$$=\frac{3.1}{a+bT_{BH}}, \tag{35}$$

where n_b, n_f and n are the respective densities of bosons, fermions, and all particles at the horizon. In the limit of high black hole temperatures ($a \ll bT_{BH} \Leftrightarrow T_{BH} > 10^4$ GeV):

$$\overline{E_f} \simeq 7.4\times 10^4 \frac{\mathrm{GeV}^2}{T_{BH}}. \tag{36}$$

This is a remarkable result since it predicts that for black holes of temperature $T_{BH} \gtrsim 100$ GeV ($M<10^{12}$ g) the effective temperature of emitted particles (that which would be inferred by observers far away from the hole) is actually lower, the higher is their temperature at the horizon. For an individual black hole, which is losing mass and hence becomes hotter, this means that its apparent temperature goes down. The word ''temperature'' is used loosely here: the spectrum is nonthermal, with a higher luminosity at low frequencies than that of a blackbody (see Fig. 10 below).

Equation (36) was derived on the assumption that the black hole horizon temperature does not change much on the time scale of particle diffusion from the horizon to the outer edge of the photosphere. Nevertheless, we expect the qualitative picture to be the same even for black holes temperatures above this limit of validity. It should also be kept in mind that we are discussing only electromagnetically interacting particles so far. The behavior of the QCD photosphere (below) is quite different.

The time development of an individual BH, based on the above results, can now be described. As far as only QED emission is concerned, a photosphere starts to develop around the black hole when it evaporates to a mass of $M \simeq 5\times 10^{12}$ g. At this point the average energy of emitted particles, instead of going up inverse proportionally to the BH mass, levels off and begins to decrease. On the other hand, the total luminosity increases, and the spectrum becomes softer than that of a black body. The outer edge of the photosphere remains at a radius of 400 fm$\sim m_e^{-1}$. However, its inner radius, $r_i \sim 700 r_h$, shrinks with the Schwarzschild horizon r_h. Eventually, if the steady-state assumption remains valid at these temperatures, the edge will cool to $\overline{E_f} \sim m_e$, when the positrons and electrons annihilate and no further cooling occurs.

To give some idea of how the results of the test particle method differ from the estimates in [7], where a nonperfect fluid model was used, we tabulate the relevant quantities in Table I, for three different BH temperatures.

C. Inside the photosphere

A more detailed picture of the plasma can be seen from the particle momenta distributions at different radii inside the photosphere. Since no significant interactions start before $r \sim 10^4 r_h$, particles move increasingly radially until the inner boundary of the photosphere. By this point they have on average undergone one interaction and their momenta begin to get randomized. Close to the end of the photosphere, the mean free path increases the radial components of the momenta again start to increase. These developments can be seen in the distributions of the transverse momenta. In Fig. 10 we show the distributions of the fraction of momentum which is transverse to the radial direction, $p_t/p = p_t/\sqrt{p_t^2+p_r^2}$, for several radii inside a sample photosphere. These figures show the overall growth in particle density as well as the shift to larger p_t as one goes from the inner boundary of the photosphere toward its interior.

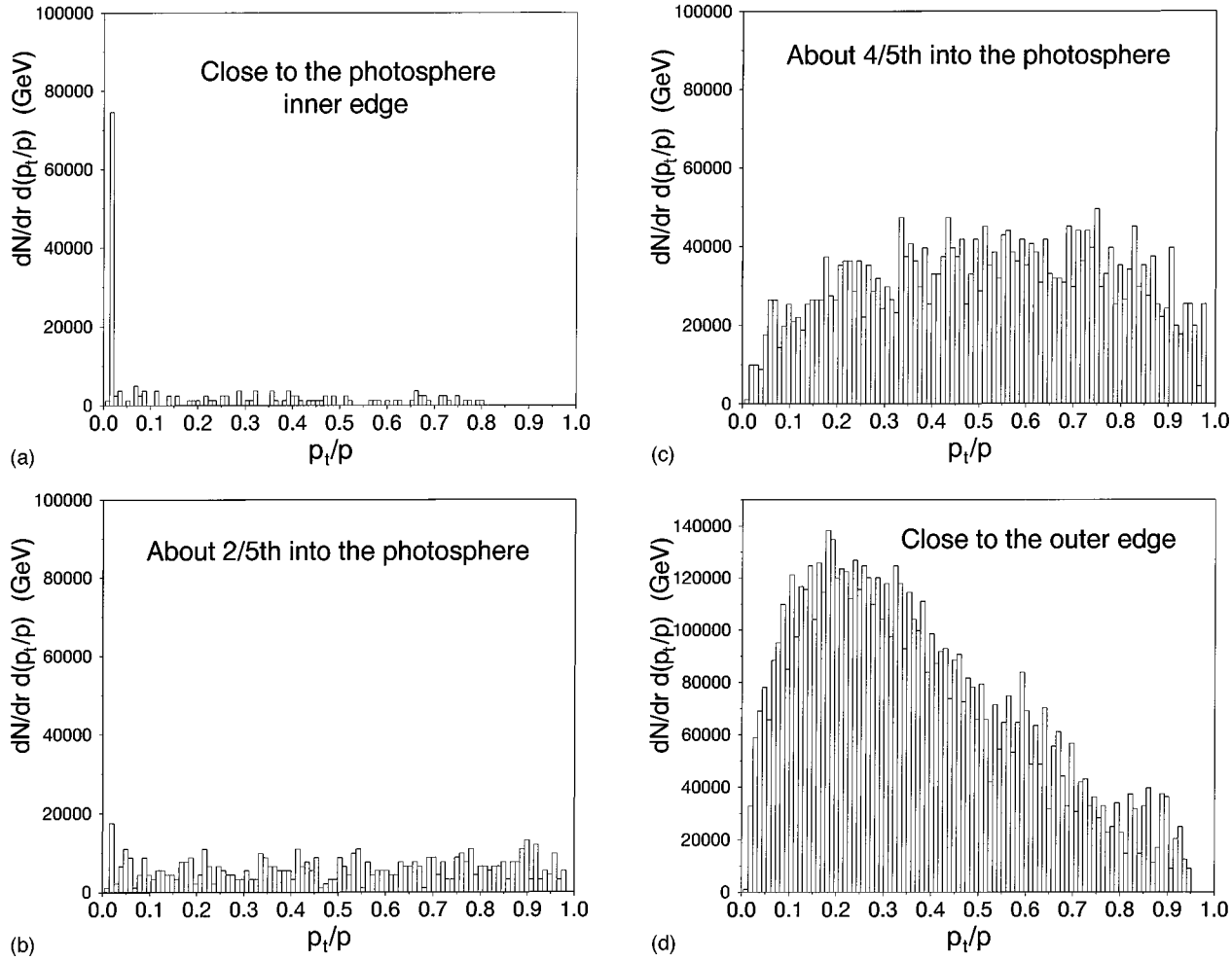

FIG. 10. Distribution of p_t/p for several radial shells in the QED photosphere of a BH with $T=1000\,\mathrm{GeV}$.

D. Spectra

Finally, we examine the particle energy spectra at the black hole horizon and at the photosphere edge (Fig. 11). The shift toward lower energies is the most significant difference between the original distribution at the horizon and those within the photosphere. The two are shown together in Fig. 12, where it can be seen that the softening in energy is accompanied by an increase in the number of particles, as is required by energy conservation.

The QED photosphere by itself serves as a kind of toy model for realistic black holes, which are also emitting quarks and gluons at the temperatures we are considering. We now turn our attention to the QCD photosphere.

TABLE I. QED photosphere parameters (temperature at horizon, inner and outer photosphere radii, and average particle energy at the outer edge of the photosphere) for several black hole temperatures obtained in test particle simulations.

T_{BH}	r_i	r_f	$\overline{E_f}$
60 GeV	1.5×10^3 fm	8.6×10^3 fm	97.0 GeV
300 GeV	30 fm	9.6×10^3 fm	79.5 GeV
1000 GeV	7.9 fm	9.6×10^3 fm	44.2 GeV

QCD photosphere

A black hole whose temperature exceeds $\Lambda_{QCD}\sim200\,\mathrm{MeV}$, thus having a mass $M_{BH}\lesssim5\times10^{14}\,\mathrm{g}$, emits quarks and gluons which, as proposed by MacGibbon and Weber in Ref. [8], fragment into hadrons, decaying in their turn into stable particles. We have modeled the interactions of the quarks and gluons before hadronization takes place. In this regime, as suggested by Heckler in Ref. [7], a quark-gluon plasma similar to the electron-photon photosphere in QED may develop, analogously changing the energy spectrum of the particles.

E. Test particle method in QCD

Our treatment does not attempt to give a detailed model of QCD interactions after hadronization begins. However, the onset of the photosphere can be established in terms of free quarks and gluons interacting with each other. We assume that hadronization occurs at a distance of $\sim\Lambda_{QCD}^{-1}$ and that no significant softening of the particle spectrum occurs after this point. Hence, we make the same test particle simulation as in QED, only with different interaction cross section,

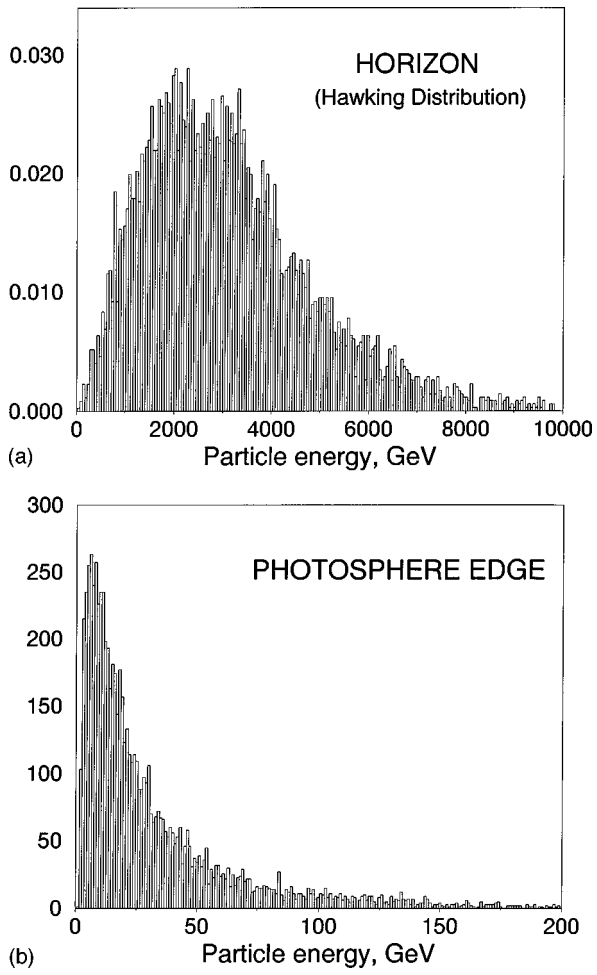

FIG. 11. Energy spectrum of a 1000 GeV (10^{11} g) black hole at the Schwarzschild horizon and near the edge of the QED photosphere.

masses, and number densities. Because of the much larger coupling constant and greater number of degrees of freedom, we expect the photosphere to develop at temperatures T_{BH} far below the critical temperature for QED, $T_c \sim 50\,\mathrm{GeV}$, and to reach higher densities than in the QED case.

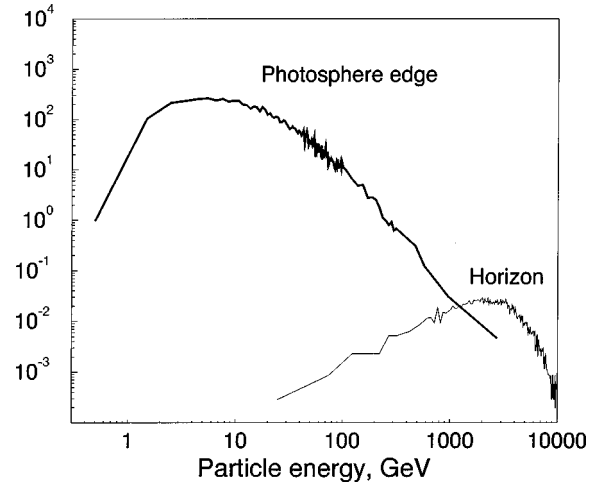

FIG. 12. Same as Fig. 11, but with the two spectra superposed.

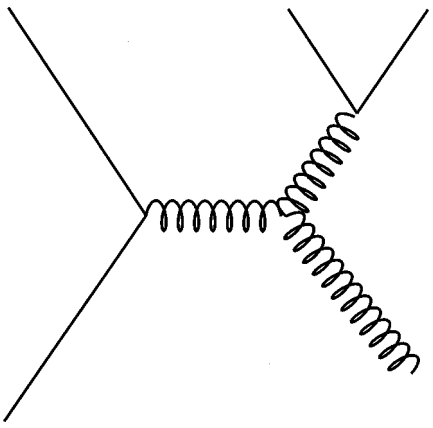

FIG. 13. Non-Abelian contribution to quark-gluon bremsstrahlung.

To investigate the photosphere in QCD, we recall that the key ingredient was the inclusion of $2 \rightarrow 3$ body interactions in the collision term of the Boltzmann equation (3). Like electrons and photons, quarks and gluons can also interact via bremsstrahlung ($qq \rightarrow qqg$) and pair production ($qg \rightarrow qq\bar{q}$). The dominant diagrams (which give large logarithms in the cross section at low momentum transfer due to t-channel propagators) are the same as for QED, Fig. 2. In addition, there are intrinsically nonabelian contributions like Fig. 13 which we do not expect to be parametrically larger than those of Fig. 2. We will therefore make the simple approximation of modeling the bremsstrahlung and pair production cross sections using the same form as in QED, but replacing the fine structure constant by α_s and the electron mass by the mass of the lightest quark:

$$\sigma_{brem}^{QCD} \simeq \frac{8\alpha_s^3}{m_{th}^2} \ln \frac{2E}{m_{th}}. \tag{37}$$

Here $m_{th} = \sqrt{m_q^2 + m_p^2}$ using the QCD plasma mass, Eq. (27), and we take m_q to be the average of the up and down quark masses, $m_q \cong 8\,\mathrm{MeV}$. Based on the previous QED results, heavier quarks are expected to make a subdominant contribution to the photosphere, since their bremsstrahlung cross sections are smaller by a factor of the mass ratio squared. The dependence of the thermal quark mass on radial distance in the photosphere was already shown in Fig. 3.

In contrast to QED, the QCD coupling constant depends strongly on energy. To leading order in perturbation theory [17],

$$\alpha_s(\mu) = \frac{12\pi}{(33 - 2n_f)\ln(\mu^2/\Lambda_{QCD}^2)}, \tag{38}$$

where in our radial evolution we take μ to be the average particle energy at a given radius, $\Lambda_{QCD} \sim 200\,\mathrm{MeV}$, and n_f ranges between 3 and 5 for the BH temperatures we are considering, depending on the number of quark species with masses less than the average energy at a given distance from the horizon.

When the effective temperature of the quark-gluon plasma becomes of order Λ_{QCD}, perturbation theory in α_s breaks down, and the quarks and gluons hadronize. This process will be discussed in Sec. IV G. At distances greater than Λ_{QCD}^{-1}, instead of a gas of quarks and gluons, we will have a plasma of pions and nucleons, which can in principle continue to cool through pion bremsstrahlung ($nn \to nn\pi$ or $\pi\pi \to \pi\pi\pi$). However the residual strong interactions of pions and nucleons are screened, relative to those of the quarks and gluons, by confinement. Also the relevant scale for the range of pion bremsstrahlung is m_π^{-1}, which is much shorter than the range of quark-gluon brehmsstrahlung. We expect these two reductions in the strength of $2 \to 3$ scattering processes to make the hadrons much less effective than quarks and gluons in perpetuating the photosphere. Thus one might anticipate that the QCD photosphere ends rather abruptly beyond distances of order Λ_{QCD}^{-1}.

To semiquantitatively investigate this post-hadronization regime, we modeled the hadron gas by replacing α_s by the pion-nucleon fine-structure constant, $f^2/4\pi \cong 0.09$, obtained from low-energy pion-nucleon scattering [18]; we also substituted the quark mass with the pion thermal mass, which we estimate analogously to Eqs. (25) and (27). The result is that hadron-hadron interactions are indeed ineffectual for prolonging the photosphere. Henceforth we simply use the hadronization criterion to determine where the photosphere ends.

F. Parameters of QCD photosphere

We have found that the QCD photosphere starts to develop for any black hole whose temperature exceeds a critical value

$$T_c \simeq 175 \text{ MeV}. \tag{39}$$

This is more than two orders of magnitude lower than the critical temperature for the QED photosphere. It agrees with the analytical estimate in [7], $T_c \sim \Lambda_{QCD}$. Recall that T_c is defined to be the temperature at which each particle on average undergoes one scattering during its outward propagation. In Fig. 14 we show the average number of scatterings per particle as a function of distance, $\mathcal{N}(r)$, at several BH temperatures. In contrast to the QED case (Fig. 5), where $\mathcal{N}(r)$ levels off at a universal value of the final radius r_f marking the end of the photosphere, in QCD r_f depends strongly on the temperature. The radius at which hadronization takes place grows with T_{BH}, which will be quantified below.

The precise definition of the final radius, r_f, differs in the QCD case from that which we used for QED: for QCD we must decide just where hadronization occurs. One can imagine several possible criteria: when the interparticle spacing $[n(r_f)]^{-1/3}$ begins to exceed Λ_{QCD}^{-1}; when the average particle energy $\overline{E}(r_f)$ becomes of order Λ_{QCD}; or when the coupling constant $\alpha_s(r_f)$ becomes of order unity. We find that all three are roughly equivalent in that the value of r_f depends only marginally on which one is used. We adopt the coupling constant criterion to define r_f in the results that follow. Figure 15 shows that r_f is well described by a logarithmic growth in the photosphere radius with the black hole temperature:

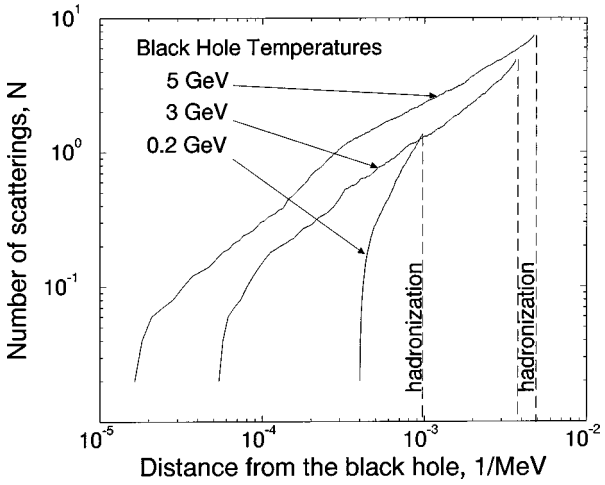

FIG. 14. Average number of scatterings $\mathcal{N}$ in QCD photosphere as a function of radius r for several black hole temperatures.

$$r_f = A + B \ln\left(\frac{T_{BH}}{1 \text{ GeV}}\right), \tag{40}$$

where $A = 3.25 \pm 0.09\,\text{GeV}^{-1} \simeq 0.65$ fm and $B = 1.45 \pm 0.06\,\text{GeV}^{-1} \simeq 0.29$fm.

QCD also differs from QED for the onset of the photosphere, whose inner radius is denoted by r_i. We find that significant QCD interactions begin quite close to the horizon: $r_i \sim r_h$ for the whole range of BH temperatures for which the QCD photosphere forms.

The parameter which best characterizes the intensity of interactions in the QCD photosphere is the total particle pro-

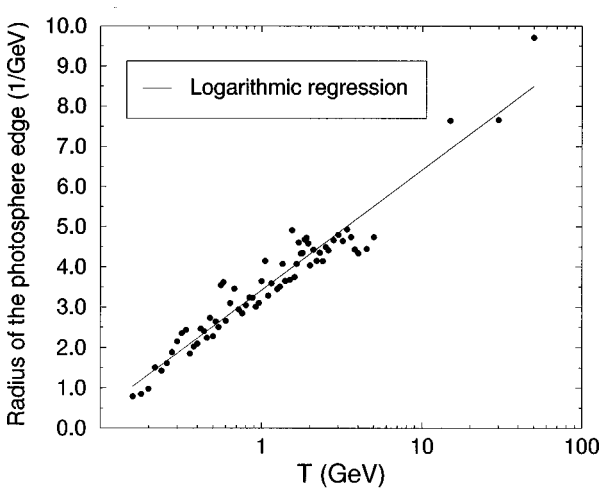

FIG. 15. Radius of the outer surface of the QCD photosphere (r_f) versus logarithm of the black hole temperature.

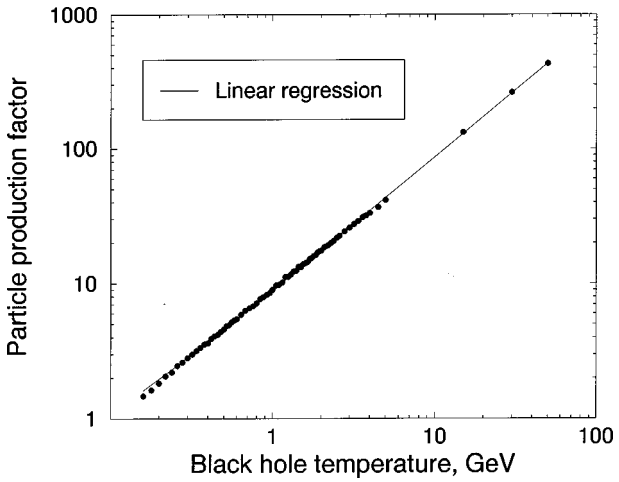

FIG. 16. Total particle production in the QCD photosphere versus black hole temperature.

duction factor, $P(T_{BH})=N(r_f)/N(r_h)$. As shown in Fig. 16, we find that it increases quite linearly with black hole temperature:

$$P(T_{BH})=(8.62\pm 0.01)\frac{T_{BH}}{\mathrm{GeV}}. \tag{41}$$

This, again, contrasts with the QED case, which displayed a noticeable quadratic dependence on T_{BH} at high temperatures.

The final spectra at the photosphere surface are not exactly thermal, but they can be fitted over most of the range where dN/dE is significant by a Boltzmann distribution,

$$\frac{dN}{dE}\propto \exp(-E/T_0), \tag{42}$$

where the effective temperature at the photosphere is independent of T_{BH}:

$$T_0=300\ \ \mathrm{MeV}. \tag{43}$$

In Fig. 17 we show the superimposed spectra at the photosphere for three different initial temperatures, $T_{BH}=1.5$, 15 and 30 GeV, along with the fit (42). The spectra are normalized to have the same maximum value so the shapes can be compared. They rise very sharply from $dN/dE=0$ at $E=0$. The actual normalization of the flux $dN/dEdt$ will be discussed below.

From our simulations at different temperatures we can reconstruct the time evolution of the QCD photosphere of an individual BH. A black hole that has reached a temperature greater than $T_c=175\,\mathrm{MeV}$, corresponding to a mass $M\lesssim 5\times 10^{14}\,\mathrm{g}$, emits quarks and gluons which almost immediately begin interacting to form a photosphere very close to the horizon, $r_h\lesssim 0.1\,\mathrm{fm}$. As the black hole temperature continues to rise, the photosphere inner radius shrinks along with the horizon ($r_i\sim r_h=1/4\pi T_{BH}$), while the outer radius grows

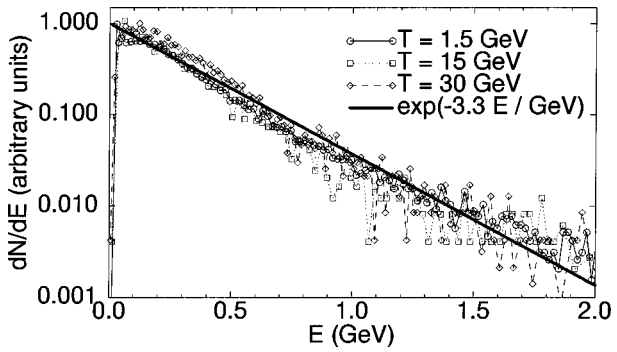

FIG. 17. Linear-log plot of QCD photosphere spectra (normalized to have same peak value) for three different horizon temperatures, and the analytic fit $dN/dE=\exp(-E/300\,\mathrm{MeV})$.

logarithmically with T_{BH}. Particles emitted from the horizon with average energy $\overline{E_i}\sim 3T_{BH}$ fragment in the photosphere into lower energy particles. The higher T_{BH}, the more particles are created (Fig. 16). The average particle energy decreases as they propagate outward, until it reaches $\overline{E_f}\sim 300\,\mathrm{MeV}$ at the photosphere edge, where hadronization occurs.

The results for the photosphere parameters for several characteristic black hole temperatures are summarized in Table II. As is evident, the average particle energy can decrease by several orders of magnitude in a QCD photosphere. How the full spectrum changes is illustrated in Fig. 18, where we show the energy distributions of the particles at the horizon and at the photosphere edge of a 1.5 GeV black hole. In this example the average energy decreases by a factor of 13, and the number of particles increases by the same factor, given by $P(1.5\,\mathrm{GeV})$ [Eq. (41)].

Of course it is not the quarks and gluons that might reach a distant observer, but rather the subsequently produced hadrons and their decay products, especially the photons. We will therefore consider the processes by which the QCD plasma creates a potentially observable gamma ray or antiproton signal.

V. POSSIBLE EXPERIMENTAL CONSEQUENCES OF THE PHOTOSPHERE

Finally we would like to see what difference the photosphere makes for observational cosmology or astrophysics. From the foregoing it is clear that the spectrum of radiation from an individual black hole near the end of its existence will be considerably softened from the usual expectation based on the Hawking flux, Eq. (1). In addition, the inte-

TABLE II. QCD photosphere parameters for several black hole temperatures obtained from the test particle simulation.

T_{BH}	$r_i\sim r_h$	r_f	$\overline{E_i}$	$\overline{E_f}$
200 MeV	2.2 fm	4.9 fm	600 MeV	300 MeV
1 GeV	0.4 fm	19 fm	3.0 GeV	300 MeV
50 GeV	0.008 fm	49 fm	156 GeV	300 MeV

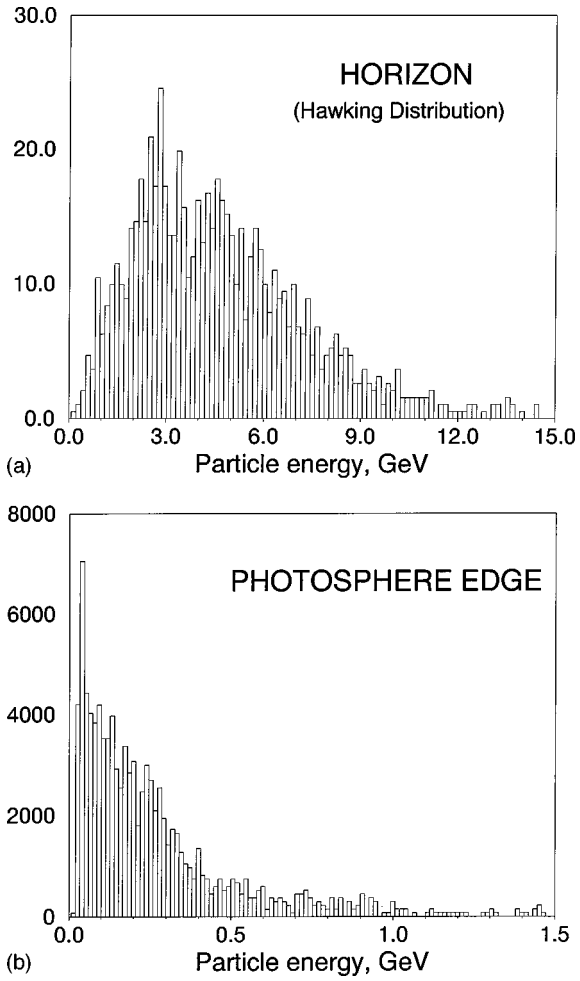

FIG. 18. Energy distribution of quarks and gluons at the horizon of a 1.5 GeV black hole and at the edge of the QCD photosphere.

grated contributions of black holes to the diffuse gamma ray or cosmic antiproton backgrounds should be shifted to lower energies. The first step is to compute how quarks and gluons in the QCD photosphere fragment into observable particles. We will then integrate the individual BH fluxes over time and over the initial mass distribution of BH's to arrive at the diffuse background fluxes.

A. Hadronization and final spectrum of QCD photosphere

Roughly speaking, the QCD interaction is perturbative ($\alpha_s<1$) when the distance between the particles is smaller than Λ_{QCD}^{-1}. This condition is satisfied in the photosphere region. At larger distances, however, vacuum fragmentation of quarks and gluons will occur, which is what happens at the photosphere edge. For an accurate calculation of the final photon spectrum, we should first compute the neutral pion flux coming from the photosphere parton distributions using a jet fragmentation code, and then the photon flux resulting from $\pi^0\rightarrow\gamma\gamma$ decays. However, following Ref. [19] we can estimate this spectrum as a convolution of the quark-gluon spectrum, available from our test particle simulation, with the pion fragmentation function [2,8] and the Lorentz-transformed spectrum of photons from π^0 decay:[2]

$$\frac{d^2N_\gamma}{dE_\gamma dt}=\int_{E_0}^{\infty}dE_\pi\frac{dg_{\pi\gamma}(E_\pi)}{dE_\gamma}\frac{d^2N_\pi}{dE_\pi dt}, \tag{44}$$

where $E_0=E_\gamma+m_\pi^2/4E_\gamma$. The number of photons of energy E_γ created by a pion moving with velocity β and decaying isotropically in its rest frame is

$$\frac{dg_{\pi\gamma}(E_\pi)}{dE_\gamma}=\frac{2}{\gamma m_\pi\beta}=\frac{2}{\sqrt{E_\pi^2-m_\pi^2}}, \tag{45}$$

where $\gamma=(1-\beta^2)^{-1/2}$. The pion flux is [8]

$$\frac{d^2N_\pi}{dE_\pi dt}=\sum_j\int_{E_\pi}^{\infty}dQ\frac{dg_{j\pi}(Q,E_\pi)}{dE_\pi}\frac{d^2N_j}{dQdt}, \tag{46}$$

where the sum is over relevant species in the plasma (quarks and gluons). For the number of pions with energy E_π produced per unit energy by each quark or gluon, we use the empirical fragmentation function [2,21]

$$\frac{dg_{j\pi}(Q,E_\pi)}{dE_\pi}=\frac{15}{16}\sqrt{\frac{Q}{E_\pi^3}}\left(1-\frac{E_\pi}{Q}\right)^2. \tag{47}$$

Lastly, $d^2N_j/dQdt$ is the quark or gluon flux at the outer edge of the photosphere. In what follows we treat quark and gluon jets equally and thus write $\Sigma_j d^2N_j/dQdt=d\dot{N}/dQ$.

Combining Eqs. (44) through (47) we obtain:

$$\frac{d^2N_\gamma}{dE_\gamma dt}=\int_{E_0}^{\infty}dE_\pi\frac{15/8}{E_\pi^{3/2}\sqrt{E_\pi^2-m_\pi^2}}\int_{E_\pi}^{\infty}dQ\sqrt{Q}\left(1-\frac{E_\pi}{Q}\right)^2\frac{d\dot{N}}{dQ}, \tag{48}$$

where $E_0=E_\gamma+m_\pi^2/4E_\gamma$.

We have calculated the integral (48) numerically for a large range of black hole temperatures. The results for one of them ($T_{BH}=50\,\mathrm{GeV}$) are presented in Fig. 19 and compared to the results obtained neglecting the photosphere, but taking into account direct quark fragmentation at the horizon and subsequent π^0 decay, as in Ref. [8]. Also shown are the spectra of photons emitted directly from the black hole (neglecting the QED photosphere) and from the QED photosphere, which just starts to form at this temperature. The actual full spectrum of a 50 GeV black hole is the addition of the two solid lines. The results are in agreement with Fig. 1 of Ref. [19], except for the QED photosphere spectrum, as discussed above.

We see that the photon flux from the QCD photosphere peaks at an energy of $m_\pi/2$; if the pions were at rest then all

[2]We differ with [19] concerning the limits of integration here. The minimum and maximum photon energies from a decaying pion boosted to energy $E_\pi=\gamma m_\pi$ are $E_\gamma=E_\pi(1\pm\sqrt{1-\gamma^{-2}})/2$. Inverting this equation implies that a photon of energy E_γ can come from pions with energies satisfying $E_\pi\geqslant E_\gamma+m_\pi^2/4E_\gamma$.

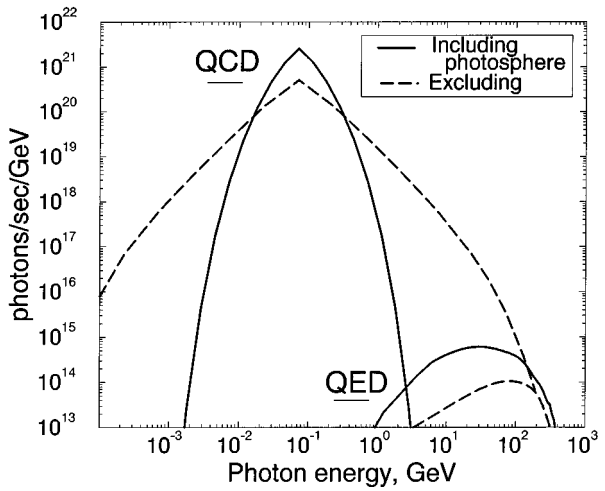

FIG. 19. Photon emission spectrum from $T=50\,\mathrm{GeV}$ ($M=2\times10^{12}\,\mathrm{g}$) black hole. Solid lines are spectra which include photospheres. Dashed lines are given for comparison and represent the results for photons from direct quark fragmentation at the horizon and subsequent π^0 decay (QCD), and for direct photon emission neglecting the QED photosphere (QED).

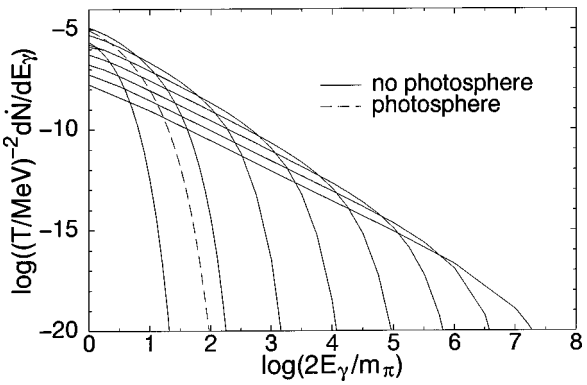

FIG. 20. Photon emission spectrum from π^0 decay for black holes, ignoring photosphere, with $T_{BH}=50\,\mathrm{MeV}$ (narrowest), increasing T_{BH} by factors of 10, up to 500 TeV (widest). Dashed curve shows the spectrum including photosphere (see text for normalization).

photons would have this energy, but E_γ is Doppler shifted by the pion motion, and the width of the distribution grows with the average energy of the pion. Figure 20 shows the photon spectra for a large range of BH temperatures in the case where the photosphere is neglected. As a function of $y\equiv\log(2E_\gamma/m_\pi)$, these spectra are symmetric under $y\to -y$. Because the total power output of the BH goes like $\int dQQd\dot{N}/dQ\sim T_{BH}^2$, it is convenient to display instead the quantity $T_{BH}^{-2}d\dot{N}_\gamma/dE_\gamma$, as we have done in Fig. 20. We fit these functions to 10th order polynomials,

$$\log_{10}(T_{BH}^{-2}d\dot{N}_\gamma/dE_\gamma)\cong\sum_i a_n|y|^n;$$

$$y\equiv\log_{10}2E_\gamma/m_\pi \tag{49}$$

whose coefficients (up to 8th order, which is still a good approximation) are given in Table III. The absolute normalization follows from the ansatz $d\dot{N}/dQ=(Q/T_{BH})^2\exp(-Q/T_{BH})/(3!)$ which we took as an approximation to the actual Hawking distribution (up to an overall normalization factor which can be computed) to obtain these functions. They will be useful later when we integrate the BH radiation over time. Although the spectra are really analytic at $y=0$, the derivative changes so quickly there that the best fit is obtained by using an odd function for $y>0$ and then letting $y\to|y|$ to cover the $y<0$ side. Also shown in Fig. 20 is the corresponding spectrum, divided by T_0^2, for the photosphere, whose parton flux is taken to be $d\dot{N}/dQ=\exp(-Q/T_0)$, where $T_0=300\,\mathrm{MeV}$. Like the nonphotosphere results, a photon spectrum computed using this distribution should be multiplied by a factor of T_{BH}^2 (for $T_{BH}>T_0$) to represent a BH with horizon temperature T_{BH}, to insure that the power output at the photosphere is equal to that at the horizon for any value of T_{BH}.

B. Diffuse gamma ray background

Finding the contribution of black hole radiation to the diffuse photon background consists of two steps: (1) first integrate the contribution of a single BH over time, and (2) integrate this result over the initial mass distribution of the individual BH's. Let us denote the time-integrated spectrum emitted by a single black hole by dN_1/dE_γ. Going from an

TABLE III. Coefficients for photon fluxes from $\pi^0\to\gamma\gamma$ used in Eq. (49).

T_{BH}	a_0	a_1	a_2	a_3	a_4	a_5	a_6	a_7	a_8
50 MeV	−5.660	−1.634	−3.055	−1.853	1.308	−1.518	−1.207	2.169	−1.596
500 MeV	−4.938	−0.973	−1.059	−0.353	1.544	−2.191	1.566	−0.710	0.189
5 GeV	−5.289	−0.822	−1.124	1.016	−0.818	0.6191	−0.418	0.195	−0.057
50 GeV	−5.882	0.237	−4.838	7.965	−8.251	5.528	−2.430	0.695	−0.125
500 GeV	−6.270	−0.795	−1.136	1.105	−0.747	0.378	−0.146	0.041	−0.008
5 TeV	−6.770	−0.777	−1.243	1.338	−0.991	0.514	−0.184	0.044	−0.007
50 TeV	−7.270	−0.735	−1.402	1.549	−1.105	0.521	−0.163	0.033	−0.004
500 TeV	−7.770	7.316	−24.23	27.72	−17.30	6.561	−1.580	0.244	−0.023
photosphere	−5.070	−1.177	−1.629	−0.515	1.506	−1.965	1.155	−0.411	0.0648

initial time t_i to the final time t_f, and accounting for the redshifting of the photons between the time of emission and the present (t_0),

$$\frac{dN_1}{dE_\gamma}=\int_{t_i}^{t_f}dtZ(t)\frac{d\dot{N}_\gamma}{dE_\gamma}[Z(t)E], \tag{50}$$

where $d\dot{N}_\gamma/dE_\gamma$ is the $\pi^0\to\gamma\gamma$ flux derived in the previous section. Notice that we must multiply both $d\dot{N}_\gamma/dE_\gamma$ and its argument by the redshift factor $Z\equiv(1+z)$. It is more convenient to integrate over the BH temperature, however. The time-temperature relation can be found by equating the rate of change of the BH mass with its power output, to obtain [3,2]

$$\frac{dT}{dt}=\overline{\alpha}(T)GT^4,$$

$$\overline{\alpha}=0.57d_{1/2}+0.23d_1, \tag{51}$$

where d_s is the number of degrees of freedom (spin, charge and color) of spin s which can be emitted by the BH at the given temperature. If we ignore the weak T-dependence of $\overline{\alpha}$, Eq. (51) gives the time-temperature relation

$$t-t_i=\frac{1}{3\overline{\alpha}}(T_i^{-3}-T^{-3}) \tag{52}$$

for a BH with initial temperature T_i at time t_i. Let us now assume that $t_i=0$ and define T_* as the initial temperature of a black hole which is disappearing today, $T_*\approx 100\,\mathrm{MeV}$. Then $t_0=1/(3\overline{\alpha}T_*^3)$, and we can write the redshift factor as

$$Z=1+z=\left(\frac{t_0}{t}\right)^{2/3}=\left(\left(\frac{T_*}{T_i}\right)^3-\left(\frac{T_*}{T}\right)^3\right)^{-2/3}. \tag{53}$$

Thus

$$\frac{dN_1}{dE_\gamma}=\int_{T_i}^{T_f(T_i)}\frac{dT}{\overline{\alpha}GT^4}Z(T)\frac{d\dot{N}_\gamma}{dE_\gamma}[Z(T)E_\gamma]. \tag{54}$$

The final temperature in this expression is given by

$$T_f=\begin{cases}T_i(1-(T_i/T_*)^3)^{-1/3}, & T_i<T_*;\\ \infty, & T_i\geqslant T_*.\end{cases} \tag{55}$$

Next we must add up the contributions from all black holes. The distribution of initial BH masses is taken to be [2]

$$\frac{dN}{dM_i}=\frac{(\beta-2)\Omega_{BH}\rho_c}{M_*^2}\left(\frac{M_i}{M_*}\right)^{-\beta}\equiv C_M M_i^{-\beta}, \tag{56}$$

where Ω_{BH} is the fraction of the critical density of the universe which is in primordial black holes, $\beta=2.5$ for the usual equation of state $p=\rho/3$, and $M_*\approx 10^{15}\,\mathrm{g}$ is the mass of a BH with $T_i=T_*$ (hence a BH which is disappearing in the present epoch). Then, trading M_i for T_i, the integral over initial BH's gives the spectrum of diffuse gamma rays as

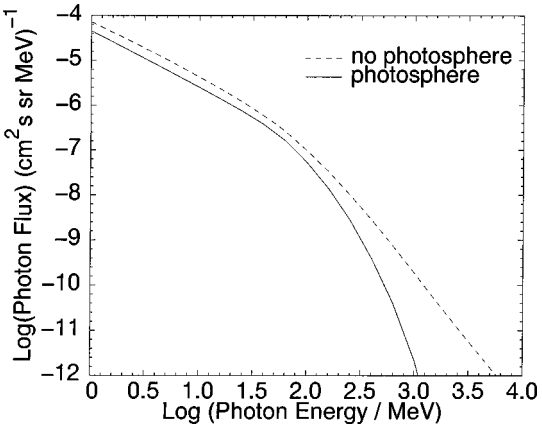

FIG. 21. Theoretical prediction for the diffuse gamma ray spectrum from decaying black holes, with and without the QCD photosphere, assuming $\Omega_{BH}=7.6\times10^{-9}h_0^{-2}$.

$$\frac{dN_\gamma}{dE_\gamma}=C_M\int_0^\infty dT_iT_i^{\beta-2}\frac{dN_1}{dE_\gamma}. \tag{57}$$

The photon flux per unit energy is dN_γ/dE_γ times the speed of light and a geometric factor, $(4\pi)^{-1}\int_0^{2\pi}d\phi\int_0^1 d(\cos\theta)\cos\theta=1/4$. We have computed this flux both with and without the QCD photosphere to see the effect of the latter. The result is shown in Fig. 21, where we have normalized the no-photosphere curve to agree with the predictions of Ref. [10] at $E=100\,\mathrm{MeV}$, for the case of $\Omega_{BH}=7.6\times10^{-9}h_0^{-2}$, which saturates the experimental limit. One sees that although the photosphere dramatically suppresses the spectrum for $E>100\,\mathrm{MeV}$, the effect is small at lower energies.

The 100 MeV energy range is the most important one for setting limits on the primordial BH contribution to the energy density of the universe, for the following reason. The theoretical prediction for the diffuse background spectrum goes like E^{-1} at low energies and E^{-3} at high energies, with $E\sim100\,\mathrm{MeV}\sim m_\pi$ being the region where the slope changes. On the other hand, the extragalactic flux measured by the Energetic Gamma Ray Experiment Telescope (EGRET) has an $E^{-2.1\pm0.03}$ energy spectrum [22], intermediate between the two theoretical slopes. Therefore as one increases Ω_{BH} from small values, the first place where the theoretical prediction comes into conflict with the observation is at the ''knee'' of the theoretical spectrum. The photosphere has only a 60% effect on the flux at these energies. In Fig. 22 we show where a line with the observed slope first encounters the predicted spectra as Ω_{BH} is increased. The intercept decreases by a factor of $10^{0.2}=1.6$ when the photosphere is taken into account; thus the bound on Ω_{BH} is only slightly weakened.

C. Antiproton background

A similar effect of the photosphere can be found in the predicted flux of antiprotons, which is interesting because of two current experiments which search for antimatter coming from cosmic sources, BESS [23] and AMS [24]. Since the

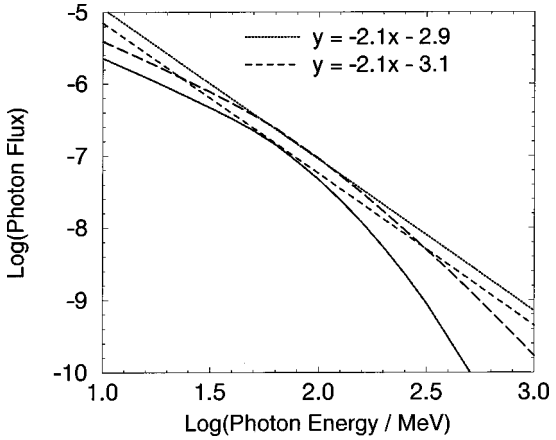

FIG. 22. Close-up of the 100 MeV region in the previous figure, showing where a line with the slope of the observed spectrum becomes tangent to each curve.

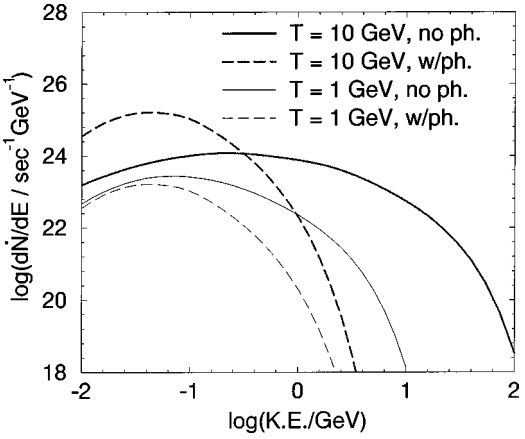

FIG. 23. Instantaneous $p,\bar{p}$ fluxes from BH's with $T_{BH}=1$ GeV (solid lines) and 10 GeV (dashed lines), including (''w/ ph.'') or neglecting (''no.ph.'') the QCD photosphere, plotted as a function of the kinetic energy.

effective temperature of the BH is limited to $\sim 300\,\mathrm{MeV}$ by the QCD photosphere, we expect a reduction in the flux of protons and antiprotons relative to predictions using the Hawking spectrum.

The computation is somewhat simpler than for photons since we only need the fragmentation of quark and gluon jets into antiprotons, with no additional subsequent decay as in the case of $\pi^0 \to \gamma\gamma$. A rough fit to the fragmentation function can be inferred from actual data for $e^+e^- \to \text{jets} \to \text{hadrons}$. Let Q be the quark or gluon energy, p_p the antiproton momentum, and $x_p = p/Q$ the momentum fraction. From Fig. 17 of Ref. [25] we find that the normalized cross section for $p,\bar{p}$ production can be fit by

$$\frac{x_p}{\sigma_{tot}}\frac{d\sigma}{dx_p} \cong \begin{cases} m_1 \ln x_p + b_1, & x_p > x_{max}; \\ m_2 \ln x_p + b_2, & x_p < x_{max}; \end{cases} \tag{58}$$

where

$$m_1 = -0.259, \quad b_1 = 0.014;$$
$$m_2 = 0.318, \quad b_2 = (m_2 - m_1)\ln x_{max} + b_1, \tag{59}$$

and the momentum fraction where the distribution peaks, x_{max}, empirically depends on the parton energy according to

$$\ln x_{max} = -0.97 \log(Q/\mathrm{GeV}) - 0.95. \tag{60}$$

Equation (58) only gives a good approximation for values such that $(x_p/\sigma_{tot})d\sigma/dx_p \gtrsim 0.03$; the tails of the distribution are better represented by a Gaussian,

$$\frac{x_p}{\sigma_{tot}}\frac{d\sigma}{dx_p} \cong F(Q)\exp\left(-\frac{\ln^2 x_{max}/x_p}{\sigma^2(Q)}\right), \tag{61}$$

where the width is supposed to depend on Q like $\sigma^2(Q) = C(\ln^{3/2} 4Q^2/\Lambda^2 - \ln^{3/2}\mu^2/\Lambda^2)$, with $\mu \cong 0.35\,\mathrm{GeV}$, $\Lambda = \Lambda_{QCD} \cong 0.2\,\mathrm{GeV}$, $F(Q)$ chosen so that $\int_0^1 dx_p (x_p/\sigma_{tot}) d\sigma/dx_p = 1$ and C being a constant. However we did not find this to be a good representation of the actual data in the vicinity of the peak, for any constant value of C. We have thus relegated the form (61) for representing the tails of the distribution, which in any case make a subdominant contribution to the final antiproton flux.

The fragmentation function is related to the cross section by

$$\frac{dg}{dE_p} = \frac{1}{\sigma_{tot}}\frac{d\sigma}{dE_p} = \frac{E}{p^2}\frac{x_p}{\sigma_{tot}}\frac{d\sigma}{dx_p}. \tag{62}$$

The $p,\bar{p}$ flux from a single black hole is then

$$\frac{d\dot{N}_p}{dE_p} = \int_{E_p}^{\infty} dQ \frac{dg}{dE_p}(Q, E_p)\frac{d\dot{N}}{dQ}. \tag{63}$$

We show the numerical results for four different cases in Fig. 23: black holes with $T=1$ GeV and $T=10$ GeV, ignoring the photosphere, and the same BH's taking the photosphere into account. We have used the results shown in Fig. 1 of Ref. [10] to fix the absolute normalization. The only effect of the horizon temperature, when the photosphere effects are included, is to multiply the distribution by a factor of $(T/T_0)^2$ for $T > T_0$, where $T_0 = 300\,\mathrm{MeV}$ is the effective temperature of the photosphere. This factor comes from demanding that the total power output of the BH is the same with or without the photosphere.

To find the diffuse antiproton flux, we should integrate over the black hole temperature and the distribution of initial masses (temperatures) as we did for photons, in Eqs. (54) and (57). The only difference is that we are interested in nonrelativistic as well as relativistic protons, so we must redshift the momentum rather than the energy. Instead of the factor $Z d\dot{N}_\gamma/dE_\gamma[ZE_\gamma]$ in Eq. (54), we get

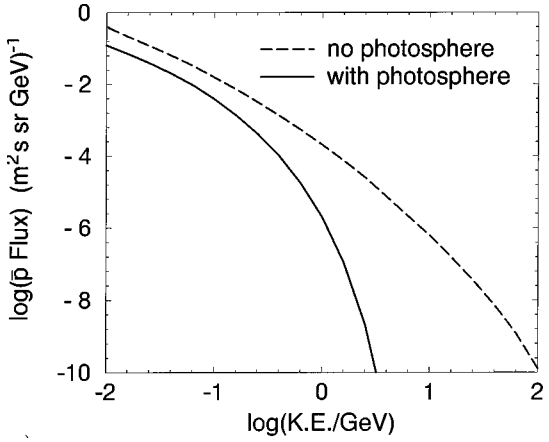

FIG. 24. Diffuse background $p,\overline{p}$ flux from integrating over time and initial distribution of BH's, as a function of the kinetic energy. Ω_{BH} is the same as in Fig. 21.

$$Z\frac{d\dot{N}_p}{dE_p}[ZE_p]\rightarrow\frac{Z^2E_p}{E_0}\frac{d\dot{N}_p}{dE_p}[E_0] \tag{64}$$

where $E_0=\sqrt{Z^2(E_p^2-m^2)+m^2}$. The result (normalized to agree with Fig. 2 of Ref. [10]) is shown in Fig. 24. Again, we take the BH density to be the maximum allowed by the gamma ray background, $\Omega_{BH}=7.6\times10^{-9}h_0^{-2}$.

The recent observations by BESS give an antiproton flux of $(8\pm2)\times10^{-3}\,\mathrm{m}^{-2}\,\mathrm{sr}^{-1}\,\mathrm{sec}^{-1}\,\mathrm{GeV}^{-1}$ at $E_p=0.2-0.3\,\mathrm{GeV}$, and higher values up to 2×10^{-2} at larger energies; thus the bound on Ω_{BH} from antiprotons is set by the low energy range of the observations. Comparison with Fig. 21 shows that the nonphotosphere prediction for the $\overline{p}$ flux is somewhat in excess of the data at these energies, suggesting that one might be able to set slightly stronger limits on Ω_{BH} using the antiproton flux rather than gamma rays. However, the predicted flux taking into account the photosphere is $10^{0.6}\cong4$ times weaker, and in better agreement with the data.

It might seem surprising that the low energy $\overline{p}$ flux is not degraded more than it is by the photosphere at kinetic energies below m_p. Apparently it is the tails of the distributions of the underlying partons which are mostly responsible for producing low-energy protons, and the largest contribution will come from black holes with temperatures somewhat below the nucleon mass. In this regime the difference between having the QCD photosphere or not is minimized.

VI. CONCLUSION

Our main results can be summarized as follows. The test-particle method of solving the Boltzmann equation, previously used for analyzing heavy ion collisions, was applied to the problem of black hole evaporation. The method was adapted to the situation of steady-state diffusion of particles emitted by a microscopic black hole. A code to simulate the bremsstrahlung and pair production interactions of the test particles was developed, leading to solutions for the particle distribution functions at any distance from the black hole horizon.

Simulation of microscopic black hole emission in both QED and QCD energy ranges corroborates the idea of photosphere formation pioneered by Heckler in [7]. We find that any black hole of mass $M\leqslant5\times10^{14}\,\mathrm{g}$ develops a cloud of interacting quarks and gluons which extends a certain distance from the black hole horizon. The evolution of such small ($r<0.08\,\mathrm{fm}$) black holes is dominated by mass loss through Hawking radiation. Part of this radiation is in free quarks and gluons which are processed in the QCD photosphere until their average energy drops to the point $\overline{E}\sim\Lambda_{QCD}$, where they hadronize into stable particles and fast-decaying pions. Another part consists of electrons, positrons and photons. Once the black hole mass drops below $M\sim2\times10^{12}\,\mathrm{g}$, these particles interact significantly enough to form another, less dense cloud at a distance about 700 times the horizon radius. This QED photosphere extends over a distance of about 400 fm, where it dissipates and emits much less energetic, but more numerous, electrons, positrons and photons.

Energy distributions of the particles leaving both photospheres were obtained and shown to greatly differ from the original nearly-thermal Hawking distributions by being softened to much lower average energies: $\overline{E}\sim300\,\mathrm{MeV}$ for QCD, and $\overline{E}$ ranging from 100 GeV (for a $10^{12}\,\mathrm{g}$ black hole) to $\sim0.5\,\mathrm{MeV}$ (for a $10^6\,\mathrm{g}$ black hole) in the QED case. We used the QCD spectra to compute the contributions of individual black holes and all BH's in the universe to potentially observable gamma ray and antiproton signals, and compared to the previous expectations based on ignoring the photosphere. In the regions where the experimental sensitivity is greatest, the photosphere lowers the fluxes by only a small factor: 1.6 for photons and 4 for antiprotons.

Our findings do not support the approximation made in Ref. [7] of treating the photosphere as a fluid. Rather we get a picture of a steadily expanding cloud of particles which never quite thermalizes, and has interactions which are primarily low in momentum transfer. This is how we interpret the fact that our Boltzmann code gives much smaller photosphere, hence much less energy degradation of particles, in the case of the QED photosphere, than claimed in [7]. This discrepancy did not appear for the QCD case because there both approaches find that the photosphere ends when hadronization begins. Furthermore we do not find a relativistically expanding photosphere, which was also claimed in [7] on the basis of the fluid approach. This led us to find larger differences in the diffuse gamma ray background between the photosphere and nonphotosphere predictions than found by Ref. [19]. The reason is that [19] undoes the energy-degrading effects of the photosphere to a large extent by boosting the distributions from the fluid frame to the observer frame, a step which is not necessary in our approach, since we always work in the latter reference frame.

It is disappointing that the observable consequences of the photosphere are small in the experimentally interesting energy ranges. If we were lucky enough to have a nearby BH reach the end of its existence however, a real experimental test might be possible, since the spectra for individual BH's have radically different characteristics with or without a

photosphere. On the theoretical side, the question of whether black hole photospheres indeed develop hinges crucially on whether the range of the bremsstrahlung interaction is really $1/m_e$ or something effectively shorter. Although the arguments supporting this claim look plausible, it is perhaps deserving of more detailed study.

ACKNOWLEDGMENTS

We wish to thank F. Halzen, K. Ragan and S. Orito for discussions or for providing helpful information. This work was supported by the Natural Sciences and Engineering Research Council of Canada.

[1] S. W. Hawking, Commun. Math. Phys. **43**, 199 (1975).
[2] F. Halzen, E. Zas, J. H. MacGibbon, and T. C. Weekes, Nature (London) **353**, 807 (1991).
[3] D. N. Page, Phys. Rev. D **13**, 198 (1976).
[4] B. J. Carr, J. H. Gilbert, and J. E. Lidsey, Phys. Rev. D **50**, 4853 (1994); R. Bousso and S. W. Hawking, *ibid.* **54**, 6312 (1996); J. S. Bullock and J. R. Primack, *ibid.* **55**, 7423 (1997).
[5] K. Jedamzik, Phys. Rev. D **55**, 5871 (1997); C. Y. Cardall and G. M. Fuller, astro-ph/9801103 (1998).
[6] F. Halzen, B. Keszthelyi, and E. Zas, Phys. Rev. D **52**, 3239 (1995).
[7] A. F. Heckler, Phys. Rev. D **55**, 480 (1997).
[8] J. H. MacGibbon and B. R. Weber, Phys. Rev. D **41**, 3052 (1990).
[9] J. Oliensis and C. T. Hill, Phys. Lett. **143B**, 447 (1984).
[10] J. H. MacGibbon and B. J. Carr, Astrophys. J. **371**, 447 (1991).
[11] G. F. Bertsch and S. Das Gupta, Phys. Rep. **160**, 191 (1988).
[12] G. M. Welke, Ph.D. thesis, McGill University, 1990.
[13] J. M. Jauch and F. Rohrlich, *The Theory of Electrons and Photons* (Springer-Verlag, New York, 1975).
[14] E. Haug, Z. Naturforsch. A **30A**, 1099 (1975).
[15] H. A. Weldon, Phys. Rev. D **26**, 2789 (1982).
[16] J. Joseph and F. Rohrlich, Rev. Mod. Phys. **30**, 354 (1958).
[17] F. Halzen and A. D. Martin, *Quarks and Leptons* (Wiley, New York, 1984).
[18] W. S. Barnes *et al.*, Phys. Rev. **117**, 226 (1960).
[19] A. F. Heckler, Phys. Rev. Lett. **78**, 3430 (1997).
[20] L. D. Landau and I. Pomeranchuk, Sov. Phys. Dokl. **92**, 553 (1953); A. B. Migdal, Phys. Rev. **103**, 1811 (1956); E. L. Feinberg and I. Pomeranchuk, Nuovo Cimento Suppl. **3**, 652 (1956).
[21] C. T. Hill, D. N. Schramm, and T. P. Walker, Phys. Rev. D **36**, 1007 (1987).
[22] EGRET Collaboration, P. Sreekumar *et al.*, astro-ph/9709257.
[23] BESS Collaboration, A. Moiseev *et al.*, Astrophys. J. **474**, 479 (1997).
[24] R. Battiston, Nucl. Phys. B (Proc. Suppl.) **65**, 19 (1998).
[25] TASSO Collaboration, M. Althoff *et al.*, Z. Phys. C **22**, 302 (1984).